INTERNATIONAL JOURNAL FOR INNOVATION EDUCATION AND RESEARCH
ISSN: 2411-2933

Journal URL: https://scholarsjournal.net/index.php/ijier

DOI: https://doi.org/10.31686/ijier.vol12.iss3.4229

A Residual-Based Numerical Viscosity Regularization Approach for Higher-Order Finite Volume Discretization of Scalar Hyperbolic Conservation Laws

Yaw Kyei
Department of decision sciences, North Carolina central university
Durham, NC 27707,

Abstract

A Space-time finite volume method is utilized to construct a parameterized family of two-step explicit higher-order schemes for scalar hyperbolic conservation laws. Utilizing a local space-time expansion of the flux-integral form of the equation error, generalized quadratures of local grid functions of the solution and the associated local source term are formulated to couple grid points within the domains of dependence and influence of new updates about the centroid of each space-time control volume. Optimal quadrature parameters for the discretization are then determined through a minimization of the error expansion to account for local space-time fluxes to all neighboring mesh points within the computational domain. Hence, a more accurate space-time descriptions of the leading numerical viscosity coefficients in the residual errors are then characterized based on the space-time coupling of the desired set of mesh points utilized in the discretization about the centroid. Consequently, the quadrature weights and the time step sizes are optimized to control and regularize the residual errors to minimize nonphysical oscillations. Numerical experiments demonstrate the effectiveness of the discretization method in minimizing the associated nonphysical oscillations in numerical solutions.

Key words. Space-time finite volume, space-time control volume, space-time discretization error, consistent higher-order accuracy, domain of dependence, flux integral, space-time residual error, equation error expansion, nonphysical oscillations

1. Introduction

In this work we utilize the finite volume method to construct a family of two-step explicit space-time discretizations for the scaler hyperbolic conservation laws with source terms. We first formulate a discretization error using generalized quadratures to approximate the flux-integral form of the equation locally about the centroid of each space-time control volume. Using a generalized quadratures of the grid functions of the solution and local source terms allow for including desired neighboring quadrature points within the domains of dependence of new updates to ensure higher conservation of local space-time fluxes. Additionally, the two-step discretization method allows for a more accurate coupling departure points with the new update

points about the centroid of the control volume and ensure higher local accuracy for the resulting schemes.

To ensure a more consistent and accurate discretization of the equation locally, a formal residual error is accurately determined to assess the effectiveness of optimizing the associated dispersion and dissipation errors for the resulting schemes. In this regard, we utilize a general weighted quadrature approximation of the integral formulation of the equation and the finite volume approach to formulate a local multivariate space-time discretization error expansion. The error expansion is then constrained by higher order derivatives of the equation to ensure higher level of conservation for local fluxes to all neighboring mesh points about the half-time centroids.

By eliminating the leading coefficients of the error expansion through a process of minimax approximation, the quadrature weights to describe the resulting schemes are determined. These closed form descriptions of the weights which describe accurate coupling of space and time scales with local physical parameters are optimized for consistency, stability and higher local accuracies. The space-time unified approach ensures that the time steps may be determined more accurately as a function of the spatial resolution, local physical parameters, and the collocation parameters to ensure that the numerical dissipation and dispersion errors for the schemes may be controlled and regulated without the need for flux limiters.

We give the general formulation of the finite volume differencing approach and then illustrate the effectiveness of the method by the construction of two-step explicit discretizations of hyperbolic conservation laws in one spatial dimension where the space-time domain [14] is two dimensional. Since space-time domains are not necessarily the cartesian products of a domain in space and a domain in time [14,15], multivariate space-time local expansions for the solution which are further constrained by higher order derivatives of the equation [10] are utilized to describe the equation error expansion. The local expansions further allow for adopting flexible configurations for the local grid-point cloud [8, 9] by utilizing all the associated space-time fluxes [10,25] to as much higher-order accuracies as possible. The structured distribution of grid points on the control volumes ensures that the resulting discretization of the equations guarantee accuracy estimates of the residual error locally and globally. Thus, the local discretization error [2] is comprehensively formulated from the generalized quadrature approximation of the flux integral form of the equation to include all directions of grid point locations on the control volume instead of just the main coordinate directions as in traditional finite difference schemes [11]. Hence, the sum of the approximation errors for all grid functions utilized in the integral formulation is first captured by the discretization error which is then minimized by determining the quadrature weights to eliminate the leading coefficients of the error. These quadrature weights form the collocations of the so-called modified equations which are optimized to improve local accuracies and for establishing space-time conditions for stability and monotonicity.

The paper is organized as follows: In Section 2, we present the space-time finite volume differencing framework for the design of the schemes by looking at the multivariate discretization of the general conservation laws in R^n. In Section 3, we apply the method to set up the generalized quadrature differencing framework for the equation error expansion aimed at achieving higher-order discretization of conservations laws in one dimension. In Section 4, leapfrog and non-leapfrog integration setups are described in space and time. In Section 5, two-step explicit three-point finite volume schemes in one spatial dimension are developed

for leapfrog and non-leapfrog integration setups. The residual errors for the schemes are analyzed through strategies for controlling and regulating nonphysical oscillations associated with numerical solutions for conservation laws. In Section 6, two-step explicit five-point finite volume schemes are presented as in Section 5. Numerical results demonstrating the accuracy and the skills of the schemes for regulating and controlling nonphysical oscillations are illustrated in Section 7. We then discuss convergence and stability of the schemes in Section 8 and provide conclusions are presented in Section 9.

2. A Space-time Finite Volume Differencing Discretization.

In this section, we present a space-time discretization framework for constructing two-step explicit schemes for the scalar hyperbolic conservation law written in the primitive form as

$$u_t + cu_x = f \quad \text{in } \Omega \times (0,T],\ x \in \Omega, \qquad (2.1)\ u(x,0) = u_0(x) \quad \text{for } x \in \Gamma,$$

through a finite volume method on a space-time cylindrical domain $\Omega \times (0,T]$ where c is the local velocity of u and $f \in L^2(0,T;L^2(\Omega))$. We use a local space-time unified framework to construct stable and conservative higher-order accurate full discretization schemes for (2.1) in a comprehensive manner that guarantees greater local accuracy improvements in time integration over semidiscretization approaches. The approach guarantees accurate tracking of flow along local characteristics and allows for local residual errors to be controlled locally by choosing the right time steps to regulate leading numerical viscosities in the residual errors. By describing local viscosity coefficients in space-time and consequently choosing time steps to match spatial resolution in order to minimize and regulate these coefficients provides degrees of freedom to better represent sharp gradients to a higher local accuracies. Furthermore, by using local solution expansion for grid function and therefore the equation error approximation, the numerical viscosity regulations and the associated errors are local.

To effectively represent and account for local space-time fluxes [4,10], we integrate (2.1) over spatio-temporal domains rather than in spatial and then temporal directions independently [21] as in traditional semi-discretization formulations. We first use the divergence theorem to rewrite (2.1) as

$$\int_{\Omega_T} u_t\,dxdt + \int_{\Omega_T} cu_x\,dxdt = \int_{\Omega_T} f\,dxdt, \qquad (2.2)$$

where Ω_T is the closure of $(a,b) \times (0,T]$.

Now, consider the two-dimensional domain Ω_T partitioned into space-time control volumes where each control volume is centered on a space-time grid point with a surrounding regular distribution of space-time grid points. Thus, each grid point has a compact cloud of quadrature points that describes the control volume overlapping [24] with grid-point distributions for neighboring control volumes. The interlocking configurations created by these overlaps allow for efficiently conserve local fluxes to neighboring points across different time levels. While in other space-time approaches [1,3,17,18], balance of fluxes is considered on the finite space-time slabs, we carry out the differencing discretization to balance local fluxes to all neighboring space-time quadrature points on the computational domain.

Following a similar characterization of the local space-time domain [18], consider a partition of the time

interval $[0,T]$ by $0 = t_0 < t_1 < \cdots < t_N = T$ and the domain $[a,b] \in \mathbb{R}$ by $a = x_0 < x_1 < \cdots < x_M = b$ such that the space-time control volume is $\mathbf{Q}^n{}_m = [x_m - h, x_m + h] \times [t_{n-1}, t_{n+1}]$, and illustrated in Figure 2.1. Each grid point $X_0(x_m, t_n)$ for instance, is a centroid of a control volume $\mathbf{Q}^n{}_m$ with a cloud of neighboring grid points $X_1(x_m + h, t_n)$, $X_2(x_m + h, t_{n+1})$, $X_3(x_m, t_{n+1})$, $X_4(x_m - h, t_{n+1})$, $X_5(x_m - h, t_n)$, $X_6(x_m - h, t_{n-1})$, $X_7(x_m, t_{n-1})$, and $X_8(x_m + h, t_{n-1})$, as depicted in Figure 2.1 where $\mathbf{Q}^n{}_m$ overlaps with control volumes centered on all the neighboring grid points.

The schemes are designed to efficiently account for the balance of local spacetime fluxes between each grid point and surrounding clouds of quadrature points in all directions and not just the coordinate directions as in traditional finite difference schemes [7]. Therefore, as the interlocking configuration to represent both local forward and backward fluxes about each centroid become more elaborate, higher accuracies and conservation are achieved by regulating the leading dissipation and dispersion coefficients to control nonphysical oscillations without the need for flux limiters.

We rewrite (2.2) into the flux integral balance form on each control volume $\mathbf{Q}^n{}_m$

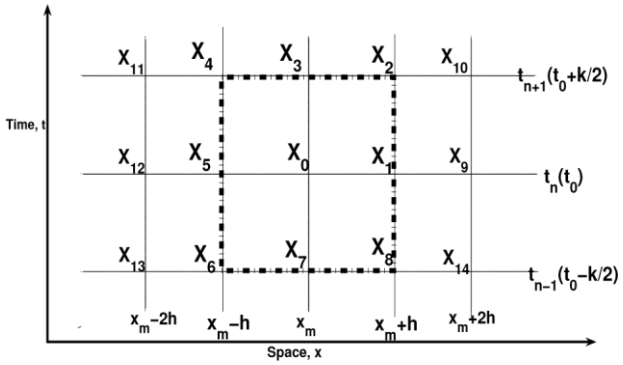

Fig. 2.1. *A space-time control volume* $\mathbf{Q}^n{}_m$ *with local uniform compact cloud of grid points with* $X_0(x_0,t_0)$ *as the centroid*

by

$$\int_{\partial \mathbf{Q}_{nm}} u \cdot \nu_t \, dx + c_{ik} \int_{\partial \mathbf{Q}_m} {}_n u \cdot \nu_x \mathrm{d}t = \int_{\mathbf{Q}_{nm}} f dx dt, \qquad (2.3)$$

where $\partial \mathbf{Q}^n_m$ is the space-time boundary of $\mathbf{Q}^n_m$, c_{ik} is speed of the conserved quantity u about the centroid, ν_t and ν_x are the unit normals in temporal and spatial directions on $\mathbf{Q}^n{}_m$. We then rewrite the temporal and spatial evaluations of (2.3) into boundary flux differencing balance form about (x_0,t_0) by

$$\underbrace{\int_{\partial_0} u dx - \int_{\partial_0} u dx}_{\text{temporal differencing}} + c_{ik} \underbrace{\left\{ \int_{\partial_0} u dt - \int_{\partial_0} u dt \right\}}_{\text{spatial differencing}} = \int_0 f dx dt. \qquad (2.4)$$

where $\partial \mathbf{Q}^n_{m t_0+k}$ represents the temporal update at time $t_0 + k$ whilst $\partial \mathbf{Q}^n_{m x_0+h}$ represents the corresponding spatial limit on the control volume. The well balanced flux differencing formulation (2.4) which is a generalization of the fundamental theorem of calculus in higher dimensions and manifolds is rewritten as

$$\int_{\partial \mathbf{Q}^{n}_{m\,t_0+k}} u\,dx = \int_{\partial \mathbf{Q}^{n}_{m\,t_0-k}} u\,dx - c_{ik}\left\{\int_{\partial \mathbf{Q}^{n}_{m\,x_0+h}} u\,dt - \int_{\partial \mathbf{Q}^{n}_{m\,x_0-h}} u\,dt\right\}$$

Time updates — Dependence grid points — spatial differencing

$$+ \int_{\mathbf{Q}_{nm}} f\,dxdt, \qquad (2.5)$$

local source term

to illustrate the similarities between our approach and other approaches [20,27].

As illustrated by the grid-point configuration in Figure 2.1, the grid points at time t^{n+1}, including X_2, X_3, and X_4, are utilized to construct the generalized weighted quadrature approximation of the new update integral $\int_{\partial \mathbf{Q}_{nmt0+k}} u dx$ while grid points at times t^{n-1} and t^n (namely X_5, X_0, X_1, X_6, X_7 and X_8) are utilized in approximating the integral $\int_{\partial \mathbf{Q}^{n}_{m\,t_0-k}} u\,dx$ on the control volume. Thus, the approximation of $\int_{\partial \mathbf{Q}_{nmt0-k}} u dx$ may be constituted from the domain of dependence grid points at times (t^n) and (t^{n-1}). Similar approximations are described for the boundary integrals

$\int_{\partial \mathbf{Q}_{nmx0+h}} u dt$ and $\int_{\partial \mathbf{Q}_{nmx0+h}} u dt$ which are utilized for the spatial flux differencing.

The collocation of the associated source term $\int_{\mathbf{Q}_{nm}} f\,dxdt$ may include sub-grid points where the quadrature parameters will be similarly determined for higher local accuracies. The degrees of freedom for constructing the discretization include the collocation weights which are to be determined to eliminate the leading terms of the equation error expansion and optimize the leading numerical viscosity coefficients of the residual errors.

The balanced flux setup (2.5) is very similar to the classical Godunov's finite volume methods including ADER approach [22,23] where $\int_{\partial \mathbf{Q}_{nmx0+h}} u dt$ and $\int_{\partial \mathbf{Q}_{nmx0-h}} u dt$ in (2.4) are represented by the numerical fluxes $F_{i+1/2}$ and $F_{i-1/2}$ respectively; finite

difference approaches where $\int_{\partial \mathbf{Q}_{nmt0+k}} u dx$ and $\int_{\partial \mathbf{Q}_{nmt0+k}} u dx$ are represented by the centroid values of u_i^{n+1} and u_i^{n-1} at t_0+k and t_0-k boundaries of the control volume.

In these different approaches [22], the approximation of the fluxes $F_{i+1/2}$ and $F_{i-1/2}$ are treated with elaborate interpolation procedures at the cell boundaries independently and as such flux limiters to regulate the flux differencing $F_{i+1/2} - F_{i-1/2}$ are needed.

In this approach, the spatial and temporal differencing are carried out in a unified manner about the centroid by using of all neighboring cloud of grid function values similar to idea behind the construction of flux limiters. Thus, the generalized quadrature approximation of the equation error for (2.5) is described as

$$E_{uik} = \sum_n \alpha_i u_i - \sum_n \beta_i u_i + c_{ik} \sum_n a_i u_i - \sum_n b_i u_i - \sum v_i f_i, \qquad (2.6)$$

$\partial \mathbf{Q}_{mt0+k}$ $\partial \mathbf{Q}_{mt0-k}$ $\partial \mathbf{Q}_{mx0+h}$ $\partial \mathbf{Q}_{mx0-h}$ $\mathbf{Q}_{nm}$

temporal residual spatial residual

where E^u_{ik} is non-zero for a finite number of quadrature points on the control volumes with quadrature weights $\{\alpha_i, \beta_i, a_i, b_i, v_i\}$ and $\{u_i, f_i\}$ as the local grid functions of u and f as defined by (2.1).

To construct the space-time expansion of the equation error (2.6) that locally enforces a more accurate higher-order relationship of local advection with time, we first utilize a multivariate expansion φ about (x_0, t_0) to describe u by

$$\phi(x_0 + x, t_0 + t) = \sum_{m=0}^{\infty} \sum_{n=0}^{\infty} \frac{1}{m!n!} \frac{\partial^{m+n} \phi}{\partial x^m \partial t^n}(x_0, t_0) x^m t^n \qquad (2.7)$$

where φ is assumed to be smooth enough and locally defined everywhere and

$$\phi(x_0, t_0) = u(x_0, t_0),$$
$$\frac{\partial^m \phi}{\partial x^i \partial t^j}(x_0, y_0) = \frac{\partial^m u}{\partial x^i \partial t^j}(x_0, y_0). \qquad (2.8)$$

Thus, any desired set of quadrature points may be included in the approximation of the flux integrals to discretize (2.6) locally. To reflect local regularities of $u(x,t)$, the coefficients φ_{xt}, φ_{tt}, φ_{xxt}, φ_{xtt}, φ_{ttt}, etc in (2.7) are replaced by φ_{xx}, φ_{xxx}, etc in order to ensure a more accurate higher-order space-time tracking of advection along local characteristics. Thus, advection accuracies along local characteristics is enforced through (2.6) and (2.9) which allow for determining the right time-steps for the flow to match spatial resolution by controlling the leading dissipation and dispersion coefficients in the residual errors. Furthermore, the source term derivatives f_x, f_t, f_{tt}, $f_{xx} f_{xt}$, f_{xxt}, f_{xtt}, etc are introduced into (2.7) through higher-order derivatives of (2.1) along characteristics given as

$$\varphi_t(x_0,t_0) = -c_0 \varphi_x(x_0,t_0) + f(x_0,t_0),$$
$$\varphi_{xt}(x_0,t_0) = -c_0 \varphi_{xx}(x_0,t_0) + f_x(x_0,t_0), \qquad (2.9)\ \varphi_{tt}(x_0,t_0) = c_{20} \varphi_{xx}(x_0,t_0) + f_t(x_0,t_0),$$
$$\varphi_{xtt}(x_0,t_0) = c_{20} \varphi_{xxx}(x_0,t_0) + f_{tx}(x_0,t_0), \text{ etc},$$

by way of the Cauchy-Kovalevskaya procedure [12,22,23] where c_0 is assumed to be locally constant about the centroid of the control volume.

For an efficient higher-order discretization, the local source term must be collocated to account for variations in the source term and solution fluxes locally. We therefore use the differential operator action on the local expansion φ in (2.7) to define the numerical local source term by

$$f(x_0+x,t_0+t)=\triangle_\kappa\left\{\sum_{m=0}^{\infty}\sum_{n=0}^{\infty}\frac{1}{m!n!}\frac{\partial^{m+n}\phi}{\partial x^m\partial t^n}(x_0,t_0)x^m t^n\right\} \qquad (2.10)$$

where 4_κ represents the action of the differential operator locally such that

$$f_0=f(x_0,t_0)=4_\kappa\varphi|_{(x_0,t_0)}:=\varphi_t(x_0,t_0)+c_{ik}\varphi_x(x_0,t_0). \qquad (2.11)$$

The expansion about the half-time centroid (x_0,t_0) ensures that quadrature points at times t_0-k and t_0+k which describe the differences between backward and forward fluxes may be captured at the same level of accuracy through the discretization of (2.4) about the centroid. The multivariate expansion ensures that all the solution approximations at the quadrature points within the domains of dependence and influence of the centroid in the resulting scheme accurately conserve local flow based on the regularities of the solution.

We now rewrite the local equation error expansion for (2.4) about each centroid based on (2.6) by

$$E_{ik}=\underbrace{\sum_{\partial\mathbf{Q}^n}\alpha_i\phi_i-\sum_{\partial\mathbf{Q}^n}\beta_i\phi_i}_{mt_0+k\quad mt_0-k}+c_{ik}\underbrace{\left\{\sum_{\partial\mathbf{Q}_{mx_0+h}}a_i\phi_i-\sum_{\partial\mathbf{Q}^n}b_i\phi_i\right\}}_{mx_0-h\quad m}-\underbrace{\sum_{\mathbf{Q}^n}v_i f_i}_{\text{temporal residual}\quad\text{spatial residual}}, \qquad (2.12)$$

where the grid functions φ_i and f_i are defined everywhere locally. The temporal residual is designed to catch higher-order numerical fluxes as a result of the time difference between the arrival point at time t_0+k and any of the departure points at times t_0 and t_0-k. Similarly, we design the spatial residual to catch higher-order numerical fluxes as a result of spatial difference between the arrival point at time t_0+k and any of the departure points at times t_0 and t_0-k.

The discretization of (2.4) may be described as a dynamic programming problem of determing $\{\alpha_i,\beta_i,a_i,b_i,v_i\}$ to minimize (2.12) subject to (2.9) and additional constraints on the quadrature weights (3.5). To preserve the integrity of the flow locally, the arrival points which are specified by the CFL number σ, are rightly determined to minimize dissipation and dispersion errors along local characteristics. Thus, the approach allows for considering and selecting the best possible ways to track numerical fluxes between each centroid and surrounding quadrature points. For explicit time integration, the parameters α_i,a_i and b_i are constrained to eliminate the implicitness at time t_0+k as described in the next Section. The formulation in (2.12) reduces to the traditional finite differencing approach when the summations are described by only the centroid values of the boundaries of the space-time control volume.

3. Generalized Quadrature Discretization. Given that the local space-time expansion $\varphi(x,t)$ in (2.7) is defined everywhere about (x_0,t_0), we describe the quadrature differencing approximation of (2.4) in the form

$$\sum_{t^{n+1}}\alpha_i\phi_i=\sum_{\{t^{n-1},t^n\}}\beta_i\phi_i-c_{ik}\left\{\sum_{x_0+h}a_i\phi_i-\sum_{\{x_0+h,x_0\}}b_i\phi_i\right\}+\sum_{\mathbf{Q}_m^n}v_i f_i, \qquad (3.1)$$

where t^{n+1} represents the new update time t_0+k in Figure 2.1 while t^{n-1} and t^n represent departure times t_0-k and t_0 respectively and similarly for the spatial differencing.

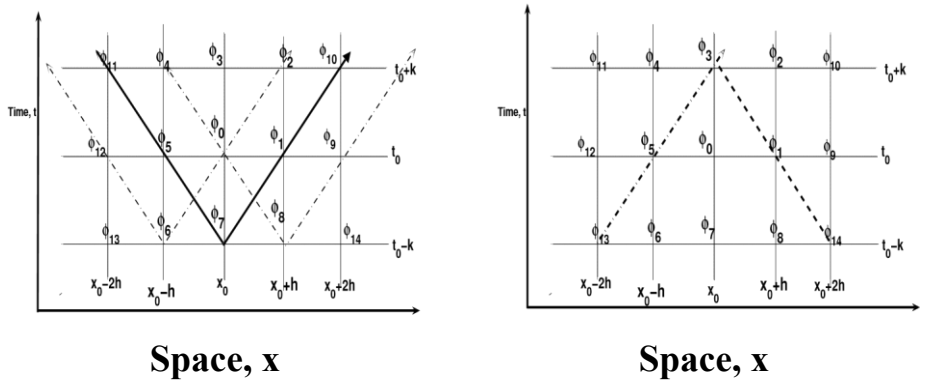

Fig. 3.1. *Grid function φ_3 is contained in* Fig. 3.2. *Domain of dependence of φ_3 inthe domains of influence of φ_{13}, φ_6, φ_7 φ_8, and cludes φ_{13}, φ_6, φ_7 φ_8, and φ_{14} at time t_0-k and φ_{14} at time t_0-k and φ_5 φ_0, and φ_1 at time t_0 φ_5 φ_0, and φ_1 at time t_0 depending on the size depending on the size of CFL number σ. of CFL number σ.*

The quadrature discretization setup of (2.4) in (3.1) differs from other work [19, 21,22] where $^{P}{}_{t_{n+1}}\alpha_i\varphi_i$ and $^{P}{}_{t_{n-1}}\beta_i\varphi_i$ are essentially the centroid values φ_3 and φ_7 at the boundary times t^{n+1} and t^{n-1} respectively on the control volume. An advantage in this approach is that $^{P}{}_{\{t_{n-1},t_n\}}\beta_i\varphi_i$ describes a weighted quadrature of solution values at two departure times t_0-k and t_0 which are within the domain of dependence of φ_3. Thus, each update φ_3, is naturally constituted from a weighted quadrature of the influencing solution values φ_1, φ_5, φ_6, φ_7, φ_8, etc as depicted in Figure 3.1 similar to the semi-lagrangian time integration method [20]. Since there are multiple departure points for each arrival point, a best CFL number is determined to regulate and minimize leading dissipation and dispersion errors which are responsible for the associated nonphysical oscillations in the numerical solutions.

As discussed above, the numerical source term f_i on the local control volume is defined such that

$$f_0 := f(t_0,x_0) = \varphi_t(t_0,x_0) + c_{ik}\varphi_x(t_0,x_0), \qquad (3.2)$$

which is consistent about the center of the control volume. The equation (3.1) is recast about (x_0,t_0) as

$$\sum_{t_0+k}\alpha_i\phi_i - \sum_{\{t_0-k,\,t_0\}}\beta_i\phi_i + c_{ik}\left\{\sum_{x_0+h}a_i\phi_i - \sum_{x_0-h,\,x_0}b_i\phi_i\right\} = \sum_{i=0}^{Ng}v_i f_i \qquad (3.3)$$

and the local discretization error E_{hk} is formulated as

$$E_{hk} = \sum_{t_0+k}\alpha_i\varphi_i - \sum_{\{t_0-k,t_0\}}\beta_i\varphi_i + c_{ik}\left(\sum_{x_0+h}a_i\varphi_i - \sum_{x_0-h,x_0}b_i\varphi_i\right) - \sum_{i=0}^{Ng}v_i f_i \qquad (3.4)$$

where Ng is the number of neighboring quadrature points that may be used in the source term collocation. To preserve the differential and integral operator properties of (2.1) in the resulting schemes, the following constraints

$$\sum_{t_0+k} \alpha_i = \sum_{t_0-k,t_0} \beta_i, \quad \sum_{x_0+h} a_i = \sum_{x_0-h,x_0} b_i, \quad \text{and} \quad \sum_{i=0} v_i = 1, \tag{3.5}$$

are enforced in the optimal sets of quadrature weights for the desired discretization design. The Cauchy-Kovalevskaya procedure [12] is the applied to replace time derivatives of φ by spatial derivatives along a characteristic line of the form

$$c_{ik}k = \sigma h \tag{3.6}$$

about the centroid of the control volume where σ is the Courant number.

As a result, the leading terms of the local discretization error expansion (3.4) about the centroid (x_0,t_0), may be reorganized as

$$\begin{aligned} E_{hk} = {} & g_0 f_0 + G_1\varphi_x + \{g_1 f_t + g_2 f_x + G_2\varphi_{xx}\}h \\ & + \{G_3\varphi_{xxx} + g_3 f_{xx} + g_4 f_{xt} + g_5 f_{tt}\}h_2 \\ & + \{g_6 f_{xxx} + g_7 f_{xxt} + g_8 f_{xtt} + g_9 f_{ttt} + G_4\varphi_{xxxx}\}h_3 + O(h_4), \end{aligned} \tag{3.7}$$

where the coefficients G_i and g_i are functions of k, h, c_{ik}, σ, and the collocation weights $\alpha_i,\beta_i,a_i,b_i,$ and v_i. Depending on the available degrees of freedom for the desired discretization, the optimization strategy is to determine the optimal sets of quadrature weights $\{\alpha_i,\beta_i,a_i,b_i,v_i\}$ to eliminate the leading terms in the error expansion E_{kh} and then regulate and control the leading coefficients of dissipation and dispersion in the associated residual errors. The resulting residual error may then be described in the form

$$\begin{aligned} R_{ik} = {} & \left\{ g_p \frac{\partial^p f}{\partial x^s \partial t^{p-s}}(c_i,d_k) + G_p \frac{\partial^{p+1}\phi}{\partial x^{p+1}}(c_i,d_k) \right\} h^p \\ & + \left\{ g_{p+1} \frac{\partial^{p+1} f}{\partial x^s \partial t^{p+1-s}}(c_i,d_k) + G_{p+1} \frac{\partial^{p+2}\phi}{\partial x^{p+2}}(c_i,d_k) \right\} h^{p+1} + O(h^{p+2}), \end{aligned} \tag{3.8}$$

where $s = 0,1,\cdots p$ and $(c_i,d_k) \in [x_0 - h,x_0 + h] \times [t_0 - k,t_0 + k]$.

Thus, R_{ik} in (3.8) describes the residual error for the discretization of the flux integral formulation of the equation (2.1) subject to its higher-order derivatives (2.9). For the numerical solution $\varphi(x,t)$ to closely mimic the unknown solution $u(x,t)$ across neighboring control volumes, the leading terms of the residual error (3.8) at each grid point must be controlled and maintained as low as possible in order for $\varphi(x,t)$ to retain the main features of $u(x,t)$. That is, the leading viscosity coefficients G_p and G_{p+1} in (3.8) must be regulated to have diminishing roles in the computational error since $\frac{\partial^{p+1}\phi}{\partial x^{p+1}}$, $\frac{\partial^{p+2}\phi}{\partial x^{p+2}}$, etc in (3.8) may be inherently large about the centroid of the control volumes for non-smooth regions of the solution. Regulating the leading viscosity coefficients to reduce the nonphysical oscillations in the numerical solutions is the essence of various viscosity stabilization techniques [13,27]. By using a general quadrature descriptions to approximate the flux integrals in the equation error expansion, a more complete and accurate coefficients of dispersion and dissipation may be obtained based on the collocations of solution values as described above. Therefore, local higher accuracies may be achieved efficiently by choosing the remaining collocation parameters to create diminishing residual errors effect on R_{ik} for the associated schemes.

We provide further details on the development of finite volume schemes by formulating a comprehensive equation error expansion, eliminating leading coefficients of the error expansion, and optimizing the

collocation weight to regulate G_p and G_{p+1} in resulting residual errors. We then give accuracy analysis of the discretizations through the leading viscosity coefficients which describe the functional relationships among h, k and σ and other collocation parameters that control associated nonphysical or Gibb's oscillations.

4. **Two-step Time Integration Designs.** By using the centroid of the control volume as the center for the equation error expansion, the new updates at time t_0+k are determined at the same level of accuracies and regularities as the departures points at times t_0-k and t_0 as described in (2.9). Thus, the new updates are only one time step away from the current time step t_0 and the discretization at each grid point is completely independent of neighboring grid points and therefore local errors don't affect accuracies at the neighboring grid points. As such, a two-time step integration here actually is a one time step from the current time and thus uses information from the two previous time steps.

We describe three general strategies for achieving explicit time discretizations for (3.3) based on (3.5) and the mesh-point configuration in Figure 3.2.

4.1. Temporal and Spatial Leapfrog Integrations Setup . Consider an implicit discretization of ${}^{R}{}_{\partial \mathbf{Q}_{nm}} \varphi \cdot \nu_t \, dx$ about the centroid as described in (3.3) by using a three-point weighted quadrature for approximating the flux integrals. The term ${}^{P}{}_{t_0+k} \alpha_i \varphi_i$ is described using a weighted quadrature of φ_2, φ_3 and φ_4 at time t_{n+1} while ${}^{P}{}_{t_0-k} \alpha_i \varphi_i$ is described as a weighted quadrature of φ_6, φ_7 and φ_8 at time t_{n-1} such that

$$\varphi_4 := \varphi_{in+1+1},\ \varphi_3 := \varphi_{ni+1},\ \varphi_2 := \varphi_{in+1+1},\ \varphi_6 := \varphi_{in+1-1},\ \varphi_7 := \varphi_{in-1},\ \varphi_8 := \varphi_{ni+1-1},$$

$$\varphi_1 := \varphi_{ni+1},\ \varphi_5 := \varphi_{ni-1},\ \varphi_0 := \varphi_{ni}. \quad (4.1)$$

Define an implicit time differencing of ${}^{R}{}_{\partial \mathbf{Q}_{nm}} \varphi \cdot \eta_t \, dx$ on the control volume in Figure 3.2 through a leapfrogging of current time step t_0 by

$$\int_{\partial \mathbf{Q}_m^n} \phi \cdot \eta_t \, dx \approx \sum_{t_{n+1}} \alpha_i \phi_i - \sum_{t_{n-1}} \beta_i \phi_i := \frac{\{\alpha_2(\phi_2+\phi_4)+(1-2\alpha_2)\phi_3\} - \{\beta_6(\phi_6+\phi_8)+(1-2\beta_6)\phi_7\}}{2k} \quad (4.2)$$

where the values φ_6, φ_7 and φ_8 are within the domain of dependence of φ_3 without solution values the centroid time of t_n. Similarly, spatial differencing over the control volume ${}^{R}{}_{\partial \mathbf{Q}_{nm}} \varphi \cdot \nu_x \, dt$ may be compactly described between time dependent boundaries at x_0-h and x_0+h in a quadrature form as

$$\int_{\partial \mathbf{Q}_m^n} \phi \cdot \nu_x \, dt \approx \sum_{x_0+h} a_i \phi_i - \sum_{x_0-h} b_i \phi_i := \frac{\{a_2(\phi_2+\phi_8)+(1-2a_2)\phi_1\} - \{b_4(\phi_6+\phi_4)+(1-2b_4)\phi_5\}}{2h}, \quad (4.3)$$

where ${}^{P}{}_{x_0+h} a_i \varphi_i$ is a weighted quadrature of φ_2, φ_8 and φ_1 while ${}^{P}{}_{x_0-h} b_i \varphi_i$ is a weighted quadrature of φ_6, φ_4

and φ_5.

Notice that the diagonal values φ_2 and φ_4 at time t_{n+1} are utilized in completing the temporal quadrature differencing (4.2) as well as the spatial differencing (4.3) which leads to an implicit discretization of (2.4). To produce explicit space-time discretization of (2.4) about (x_0,t_0) and to time-match the spatial approximation, the approximations (4.2) and (4.3) are unified by matching temporal and spatial advection at the diagonal locations such that

$$a_2 = -\frac{c_{ik}h}{k}\alpha_2 = -\frac{c_{ik}h}{k}\nu, \text{ and } b_4 = \frac{c_{ik}h}{k}\alpha_2 = \frac{c_{ik}h}{k}\nu, \tag{4.4}$$

where c_{ik} is the local value of c at the centroid. Thus, flow to the arrival locations of φ_2 and φ_4 are determined as a function of φ_3 and the other departure points through the parameter ν as indicated in (4.4). In traditional finite differencing, the weights α_2 and β_6 for the quadrature differencing of the transient term u_t in (4.2) are assumed to be zero.

4.2. Spatial Leapfrog with Temporal Non-Leapfrog Integrations Setup . By utilizing all grid points at times t_0 and t_0-k within the domain of dependence of φ_3 as possible independent updating points, we rewrite the time differencing to include solution values at both times t_0 and t_0-k for the discretization of $\int_{\partial\mathbf{Q}_{nm}}\varphi\cdot\nu_t\,dx$ in line with the second fundamental theorem of calculus as

$$\sum_{i=2}^{4}\alpha_i\phi_i - \left\{\sum_{i=0}^{1}\beta_i\phi_i + \sum_{i=5}^{8}\beta_i\phi_i\right\} + c_{ik}\left\{\sum_{i=1}a_i\phi_i - \sum_{i=1}b_i\phi_i\right\} = \sum_{i=0}^{n_i}v_i f_i, \tag{4.5}$$

where

$$\sum_{i=2}^{4}\alpha_i = \sum_{i=6}^{8}\beta_i + \beta_0 + \beta_1 + \beta_5, \quad \sum_{i=1}a_i = \sum_{i=1}b_i, \quad \sum_{i=0}^{n_i}v_i = 1. \tag{4.6}$$

The conditions in (4.6) guarantee that the discretized equation remains consistent with the differential and integral formulations of the equation necessary for numerical conservation about each centroid.

4.3. Non-Leapfrog Integrations Setup in Time and Space. In the context of spatial integration, we consequently consider a full quadrature difference for $\int_{\partial\mathbf{Q}_{nm}}\varphi\cdot\nu_x\,dt$ incorporated in the (3.1) set-up as

$$\sum_{i=2}^{4}\alpha_i\varphi_i - \left(\sum_{i=0}^{1}\beta_i\varphi_i + \sum_{i=5}^{8}\beta_i\varphi_i\right) + c_{ik}\left(\sum_{1,2,8}a_i\varphi_i - \sum_{0,3,7}b_i\varphi_i - \sum_{4}b_i\varphi_i\right) = \sum_{i=0}^{n_i}v_i f_i, \tag{4.7}$$

where

$$\sum_{i=2}^{4}\alpha_i = \sum_{i=6}^{8}\beta_i + \beta_0 + \beta_1 + \beta_5, \quad \sum_{i=1}a_i = \sum_{i=1}b_i, \quad \sum_{i=0}^{n_i}v_i = 1. \tag{4.8}$$

5. Two-step Explicit Three-Point Finite Volume Schemes. In this section we discuss parameterized families of schemes for (2.4) based on a partial or a full utilization of departure point grid functions in constituting the new update value φ_3 at time $t_0 + k$ using three-point quadratures as illustrated in Figures 5.1 and 5.2 respectively.

For schemes based on Figure 5.1, the centroid mesh value φ_0 is not utilized in constituting the new update φ_3 indicating a partial leapfrogging in both space and time integrations. However, in Figure 5.2, the discretization uses φ_0 in updating φ_3 which through variations of leapfrogging in just space or time integrations but not both.

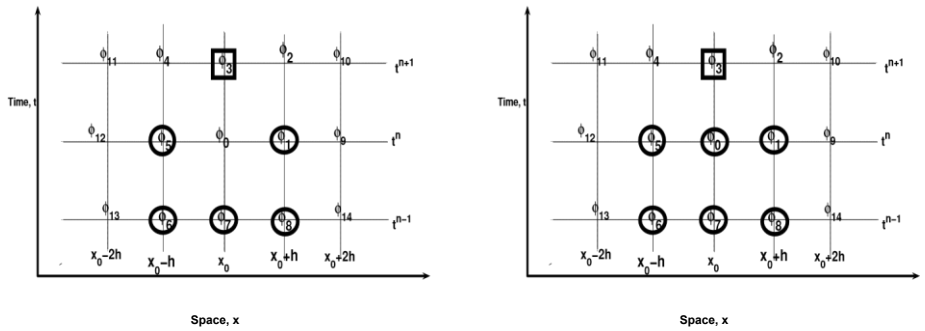

Fig. 5.1. *New update φ_3 is constituted from* Fig. 5.2. *New update φ_3 is constituted departure point values $\{\varphi_6,\varphi_7,\varphi_8\}$ and $\{\varphi_1,\varphi_5\}$ from departure point values $\{\varphi_6,\varphi_7,\varphi_8\}$ and at times t_{n-1} and t_n respectively. $\{\varphi_1,\varphi_0,\varphi_5\}$ at times t_{n-1} and t_n respectively.*

5.1. Temporal and Spatial Leapfrog Three-Point Schemes. Consider a general class of two-step explicit discretization framework where the future update φ_3 at time t^{n+1} is constituted in time from a quadrature of the three grid point values at time t^{n-1}. In determining the quadrature weights for the discretization by eliminating the leading terms of the error expansion (3.7), two additional contributions are required based on the derivative and integral conditions described in (4.6) at the centroid time t^n level as depicted in Figure 5.1.

For a second order accurate expansion of the equation error (3.7) along local characteristics (3.6), a parameterized family of two-step explicit schemes is derived as

$$\frac{1-2\nu}{2k}\phi_3 = \frac{1-2\alpha}{2k}\phi_7 + \frac{(\alpha+\nu)(\phi_6+\phi_8)-2\nu(\phi_5+\phi_1)}{2k} - c_{ik}\frac{\phi_1-\phi_5}{2h} \qquad (5.1)$$
$$+\nu c_{ik}\frac{\phi_1-\phi_5-(\phi_8-\phi_6)}{2h} + h\frac{(\alpha-\nu)\{(\phi_1-\phi_5)-(\phi_8-\phi_6)\}}{4c_{ik}k^2} + F_{32},$$

where the quadrature weight parameters ν and α are to be determined to control and regulate the leading viscosity coefficients of the resulting residual error. For a well-balanced discretization of (2.4), the local space-time source term collocation on the control volume F_{32} is determined as

$$\begin{aligned} F_{32} = {} & \frac{4f_0+f_3+f_7}{6} + \alpha\frac{(2f_3-f_2-f_4)-4(2f_0-f_1-f_5)-3(2f_7-f_6-f_8)}{24} \\ & -\nu\frac{4(f_2+f_4)-2f_3-6f_7-13(2f_0-f_1-f_5)}{12} - c_{ik}^2k^2(1-3\nu)\frac{2f_0-f_1-f_5}{6h^2} \\ & +(\nu-\alpha)h\frac{5(f_8-f_6)+8(f_1-f_5)-(f_2-f_4)}{48c_{ik}k} \\ & +(1-3\nu)c_{ik}k\frac{2f_0+f_4+f_8-(f_3+f_7+f_1+f_5)}{12h}. \end{aligned} \qquad (5.2)$$

The leading terms of the resulting residual error about the centroid for (5.1) is given as

$$R_{ik} = c_{ik}R_3\frac{\partial^3\phi}{\partial x^3}h^2 + \left(c_{ik}R_4\frac{\partial^4\phi}{\partial x^4} + \frac{\nu\sigma^3}{12c_{ik}^3}\frac{\partial^3 f}{\partial t^3} + \sigma\frac{(\nu+\alpha)}{6}\frac{\partial^3 f}{\partial x^3}\right)h^3 + c_{ik}R_5\frac{\partial^5\phi}{\partial x^5}h^4 + O(h^4), \tag{5.3}$$

where σ is the CFL number and

$$R_3 = \frac{2(1-\sigma^2) - 3\nu(3-2\sigma^2) - 3\alpha}{12}, \quad R_4 = \frac{\alpha - \nu - 2\nu\sigma^2(2\sigma^2-1) - 4\sigma^2\alpha}{24\sigma}$$
$$R_5 = \frac{2\sigma^4(5\nu-1) - 5\sigma^2(3\alpha+\nu) + 2 - 20\nu}{120}. \tag{5.4}$$

Notice that the scheme (5.1) reduces to the traditional leapfrog scheme for (2.1) with $\alpha = 0$ and $\nu = 0$, in which case time-updates for φ_3 from spatially different locations on the control volume including $\varphi_1,\varphi_5,\varphi_6,\varphi_8$ have been eliminated along with all the dissipative coefficients R_4, R_6, etc in (5.3). Thus, as a consequence of $\alpha = 0$ and $\nu = 0$ in (5.1), φ_3 lacks local advection time-updates along local characteristics from the neighboring grid points within the computational domain and local conservation is compromised. Consequently, the only available option for controlling the sizes of the dispersion error coefficients R_3, R_5, etc is to choose σ close to one. Hence, dissipation error may be described as numerical errors resulting from the use of neighboring collocation points for constructing simulation updates while dispersion errors may be described as numerical errors generated when simulation updates do not match the physical characteristics of the solution.

On the other hand, the accuracies of the approximation of (2.2) as given in (5.1) may actually be determined by the leading dispersion error coefficients R_3 and R_5 as well as the dissipation error coefficients R_4 and R_6 as illustrated by the residual error (5.3). That is, higher local accuracies may be achieved by controlling and regulating the leading viscosity coefficients by choosing the remaining parameters ν and α appropriately. These parameters describe the relative influences of the solution values at the departure times t^{n-1} and t^n on φ_3 subject to the resulting diminishing conditions that may be imposed on the residual error (5.3) for minimizing the errors due to numerical dissipation and dispersion.

To control the associated nonphysical oscillations, the leading viscosity coefficients R_3 and R_4 need to be regulated to reduce the fluctuations of φ_{xxx} and φ_{xxxx} in the computational errors. Hence determining these viscosity coefficients accurately based on the collocation points utilized for the scheme may be very essential in order to efficiently to control the oscillations without the use of flux limiters.

Strategies to Regulate Nonphysical Oscillations. Multiple approaches for choosing σ, ν and α may be devised to regulate these errors of dispersion and dissipation in the resulting schemes. We analyze some approaches based on the functional relationships of σ, ν and α with leading viscosity coefficients below:

1. **Option One:**

The parameters α and ν may be determined as a function of σ to eliminate R_3 and R_4 in (5.3) such that

$$\nu = \frac{4\sigma^2-1}{9\sigma^2-6}, \quad \alpha = \frac{2\sigma^4 - 4\sigma^2 - 1}{9\sigma^2 - 6}, \tag{5.5}$$

where the new leading dispersion and dissipative error coefficients respectively become

$$R_5(\sigma) = c_{ik}\frac{(\sigma^2-4)(\sigma^2-1)(4\sigma^2-1)}{360(2-3\sigma^2)}, \tag{5.6}$$

and

$$R_6(\sigma) = c_{ik}\frac{\sigma(\sigma^2-4)(\sigma^2-1)(4\sigma^2-1)}{1080(2-3\sigma^2)}, \tag{5.7}$$

with their functional profiles displayed in Figure 5.3 and Figure 5.4 respectively.

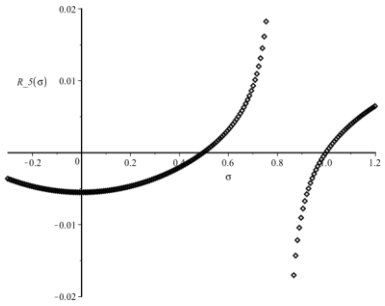

FIG. 5.3.

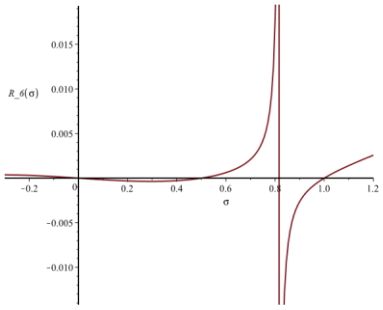

FIG. 5.4.

Thus, both local dispersion and dissipation errors may be controlled by choosing α and ν appropriately. By choosing α and ν as in (5.5), the scheme (5.1) becomes locally fourth-order accurate and since the signs of the numerical estimates of φ_{xxxxx} and φ_{xxxxxx} are unknown, the best way to control their effect on computational error and thus regulate nonphysical oscillations may be to choose σ to render both R_5 and R_6 less sensitive and as small as possible close to $\sigma = 0.5$ as depicted in Figures 5.3 and 5.4.

2. **Option Two:**

Instead of eliminating R_3 and R_4 outright as described in option one above, the parameters α and ν may be determined as a function of σ, R_3 and R_4 to regulate the size and sign of the viscosity coefficients R_3 and R_4 such that

$$\alpha = \frac{6R_3(2\sigma^4-4\sigma^2-1)+36R_4\sigma(3-2\sigma^2)}{3c_{ik}(\sigma^2-1)(3\sigma^2-2)} + \frac{(2\sigma^4-4\sigma^2-1)}{3(3\sigma^2-2)}$$
$$\nu = \frac{6R_3(4\sigma^2-1)-36R_4\sigma}{3c_{ik}(\sigma^2-1)(3\sigma^2-2)} + \frac{(4\sigma^2-1)}{3(3\sigma^2-2)}. \tag{5.8}$$

3. **Other Options:**

Various other options may be pursued such as just regulating the coefficients of the leading even-ordered derivatives of φ in the residual error [5,27]. For instance, by determining α to eliminate just R_3 as:

$$\alpha = \frac{2}{3} - 3\nu + \frac{k^2c^2}{3h^2}(6\nu-2), \tag{5.9}$$

the leading viscosity coefficients R_4 and R_5 become

$$R_4(\sigma,\nu) = c_{ik}\frac{(1-\sigma^2)(\sigma^2(9\nu-4)+1-6\nu)}{36\sigma} \tag{5.10}$$

$$R_5(\sigma,\nu) = c_{ik}\frac{(1-\sigma^2)(\sigma^2(10\nu-4)+1-10\nu)}{120} \tag{5.11}$$

with profiles as displayed in Figures 5.5 and 5.6 that show feasible regions for selecting σ and ν and the corresponding achievable sizes for R_4 and R_5.

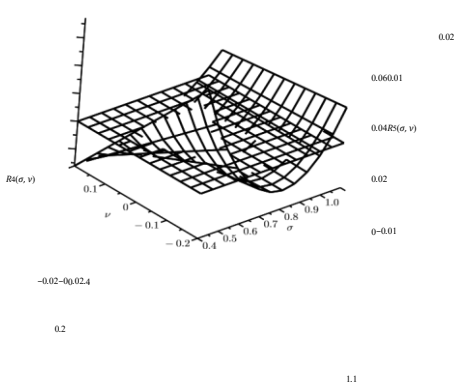

Fig. 5.5.

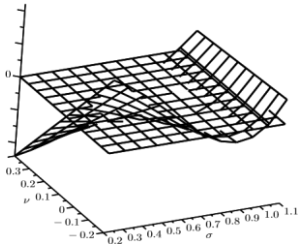

Fig. 5.6.

Additionally, by choosing α as in (5.9), both R_4 and R_5 may easily be regulated by determining ν for a given value of σ to control the signs and sizes of both R_4 and R_5 to be positive and small.

5.2. Spatial Leapfrog and Temporal Non-Leapfrog Schemes. In this section, we demonstrate the flexibility of the approach in constructing a temporal discretization of the equation using three grid points at both times t^n and t^{n-1} to update φ_3 in time as illustrated in Figure 5.2 but leapfrog the centroid in spatial integration. To utilize all grid functions within the domain of dependence of φ_3, we modify the approximation of the flux integrals given in (3.1) as

$$\sum_{i=2}^{4}\alpha_i\phi_i-\left(\sum_{i=0}^{1}\beta_i\phi_i+\sum_{i=5}^{8}\beta_i\phi_i\right)+c_{ik}\left\{\sum_{i=1}a_i\phi_i-\sum_{i=1}b_i\phi_i\right\}=\sum_{i=0}^{n_i}v_if_i,\qquad(5.12)$$

subject to the conditions

$$\sum_{i=2}^{4}\alpha_i=\sum_{i=6}^{8}\beta_i+\beta_0+\beta_1+\beta_5,\qquad\sum_{i=1}a_i=\sum_{i=1}b_i,\qquad\sum_{i=0}^{n_i}v_i=1\qquad(5.13)$$

where n_i is the total number of quadrature points to be utilized in discretizing the local source term about (x_0,t_0). Again, the conditions in (5.13) guarantee that the resulting schemes remain consistent with the differential and integral operator properties of the equation necessary for numerical conservation about each centroid.

The resulting parameterized set of two-step explicit schemes to update φ_3 on the control volume is determined as

$$\begin{aligned}\frac{1-2\nu}{2k}\phi_3=&\frac{1-2\alpha}{2k}\phi_7-c_{ik}\frac{3(\phi_1-\phi_5)+(\phi_8-\phi_6)}{6h}-c_{ik}^2\frac{k(2-6\nu)(\phi_1+\phi_5-2\phi_0)}{6h^2}\\&+\frac{3(\alpha+\nu)(\phi_6+\phi_8)+(4-6\alpha-18\nu)\phi_0+(3\alpha+3\nu-2)(\phi_1+\phi_5)}{6k}\\&-\frac{k(1-3\nu-3\alpha)((\phi_1-\phi_5)-(\phi_8-\phi_6))}{6ck^2}+F_{33},\end{aligned}\qquad(5.14)$$

where F_{33} is the associated quadrature discretization of the source term on the control volume. The resulting local residual error for (5.14) is

$$\begin{aligned}R_{ik}=&c_{ik}R_4\frac{\partial^4\phi}{\partial x^4}h^3+\frac{\sigma(\nu+3\alpha+2\sigma^2\nu)}{12}\frac{\partial^3 f}{\partial x^3}h^3+\frac{\nu\sigma^3}{12c_{ik}^3}\frac{\partial^3 f}{\partial t^3}h^3\\&+c_{ik}R_5\frac{\partial^5\phi}{\partial x^5}h^4+O(h^4),\end{aligned}\qquad(5.15)$$

where

$$R_4 = -\frac{(1-\sigma^2)(\sigma^2(3\nu-2)-1+3\nu+3\alpha)}{36},\ R_5 = \frac{(1-\sigma^2)(15\nu+15\alpha-2\sigma^2-7)}{360}$$

and σ, ν and α are to be determined to regulate the residual error.

Strategies to Regulate Nonphysical Oscillations. Again, multiple approaches for choosing σ, ν and α may be similarly devised to regulate these errors of dispersion and dissipation in the resulting schemes as:

1. **Option One:**

   The parameters α and ν may be determined as a function of σ to eliminate R_3 and R_4 such that

$$\nu = \frac{2(4\sigma^2-1)}{15\sigma^2} \qquad \alpha = \frac{2\sigma^4-\sigma^2+2}{15\sigma^2} \tag{5.16}$$

   with

$$R_6 = -c_{ik}\frac{(\sigma^2-4)(\sigma^2-1)(4\sigma^2-1)}{10800\sigma} \tag{5.17}$$

$$R_7 = -c_{ik}\frac{\sigma(\sigma^2-4)(\sigma^2-1)(4\sigma^2-1)}{37800}. \tag{5.18}$$

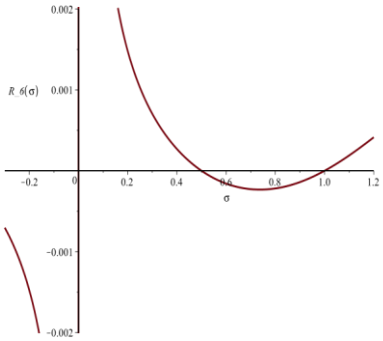

FIG. 5.7.

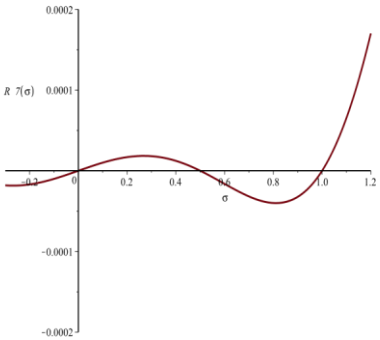

FIG. 5.8.

   In this case, as choices of σ approach $\frac{1}{2}^-$, values of ν approach 0^-, values of α approach 0^+ and the leading viscosity coefficients R_5 and R_6 stay positive and significantly reduces Gibbs phenomena in numerical solutions with discontinuities.

2. **Option Two:**

   Alternatively, the parameters α and ν may be determined as a function of σ to control the size of the viscosity coefficients R_3 and R_4 such that

$$\begin{aligned}\alpha &= \frac{180\sigma R_4 - 360R_5(\sigma^2+1)}{15c_{ik}\sigma^2(\sigma^2-1)} + \frac{2\sigma^4-\sigma^2+2}{15\sigma^2}\\ \nu &= \frac{360R_5 - 180R_4\sigma}{15c_{ik}\sigma^2(\sigma^2-1)} + \frac{2(4\sigma^2-1)}{15\sigma^2}.\end{aligned} \tag{5.19}$$

3. **Other Options:**

   Again, other options as discussed for (5.1) may be pursued.

5.3. A Non-leapfrog Spatial Integration . In this section, consider a nonleapfrog integration to utilize all departure points for both space and time where we describe the spatial and temporal differencing across the centroid of the control volume by

$$\sum_{i=2}^{4} \alpha_i \varphi_i - \sum_{i=0}^{1} \beta_i \varphi_i - \sum_{i=5}^{8} \beta_i \varphi_i - \sum_{i=13}^{14} \beta_i \varphi_i$$

$$+c_{ik}\left(\sum_{i=8,1,2} a_i\phi_i - \sum_{i=3,0,7} b_i\phi_i - \sum_{i=4,5,6} b_i\phi_i\right) = \sum_{i=0}^{n_i} v_i f_i \quad (5.20)$$

where

$$\sum_{i=2}^{4}\alpha_i = \sum_{i=5}^{8}\beta_i + \beta_0 + \beta_1 + \beta_{13} + \beta_{14},\ \sum_{i=1} a_i = \sum_{i=1} b_i,\quad \sum_{i=0}^{n_i} v_i = 1 \quad (5.21)$$

A parameterized family of schemes which may be determined from the constrained minimization process is

$$\begin{aligned}\left(\frac{1}{2k} - \frac{\nu}{k} - \frac{c_0\rho}{2h}\right)\phi_3 = {} & \frac{(2-6\nu)(\phi_6+\phi_8) + (18\nu-1)\phi_7 - 6\nu(\phi_1+\phi_5)}{6k} \\ & + c_0\frac{(\nu-1)(\phi_1-\phi_5) - \nu(\phi_8-\phi_6) - \rho(\phi_3+\phi_7-2\phi_0)}{2h} \\ & + h\frac{(1-6\nu)(\phi_1-\phi_5) - (2-12\nu)(\phi_8-\phi_6-2\phi_7)}{6c_0k^2} \\ & + kc_0^2\frac{3\rho(\phi_1-\phi_5) - 3\rho(\phi_8-\phi_6) - (2-6\nu)(\phi_6+\phi_8-2\phi_7)}{12h^2} \\ & + kc_0^2\frac{(3\nu-1)(\phi_6+\phi_8-2\phi_7) - (3\nu-1)(\phi_1+\phi_5-2\phi_0)}{6h^2} \\ & + \rho\, k^2c_0^3\frac{(\phi_6+\phi_8-2\phi_7) - (\phi_1+\phi_5-2\phi_0)}{4h^3} + F_{302}, \end{aligned} \quad (5.22)$$

where ρ provides a spatial differencing across the centroid in a way different than (5.14) but utilizes the same grid points and F_{302} is the associated source term collocation.

The resulting local residual error for (5.22) is

$$R_{ik} = c_{ik}R_4\frac{\partial^4\phi}{\partial x^4}h^3 + \frac{\nu\sigma^3}{12c_{ik}^3}\frac{\partial^3 f}{\partial t^3}h^3 + c_{ik}R_5\frac{\partial^5\phi}{\partial x^5}h^4 + O(h^4), \quad (5.23)$$

where

$$R_4 = -\frac{(\sigma^2-1)(3\rho\sigma^3 + 3\sigma^2(2\nu-1) - 6\nu + 1)}{36\sigma},$$
$$R_5 = -\frac{(\sigma^2-1)(15\rho\sigma^3 + 2\sigma^2(15\nu-7) - 60\nu + 6)}{720}$$

and σ, ν and ρ are to be determined to regulate the residual error.

Strategies to Regulate Nonphysical Oscillations. Again, multiple approaches for choosing σ, ν and α may be similarly devised to regulate these errors of dispersion and dissipation in the resulting schemes as:

1. **Option One:**

   Again, the parameters ρ and ν may be determined as a function of σ to eliminate R_3 and R_4 such that

$$\nu = \frac{1}{30} + \frac{1}{30}\sigma^2 \qquad \rho = \frac{15\sigma^2 - \sigma^4 - 4}{15\sigma^3} \quad (5.24)$$

   where

$$R_6 = -c_{ik}\frac{(\sigma^2-4)(\sigma^2-1)(4\sigma^2-1)}{10800\sigma} \tag{5.25}$$

$$R_7 = -c_{ik}\frac{(\sigma^2-4)(\sigma^2-1)(4\sigma^2-1)}{37800} \tag{5.26}$$

with similar profiles as in Figures 5.7 and 5.8 above.

2. **Option Two:**

Alternatively, the parameters ρ and ν may be determined as a function of σ to control both viscosity coefficients R_4 and R_5 such that

$$\begin{aligned}\rho &= \frac{180\sigma R_4(\sigma^2-2)-720R_5(1-\sigma^2)}{15c_{ik}\sigma^3(\sigma^2-1)}+\frac{15\sigma^2-\sigma^4-4}{15\sigma^3}\\ \nu &= \frac{720R_5-180R_4\sigma}{30c_{ik}(\sigma^2-1)}+\frac{1}{30}+\frac{1}{30}\sigma^2.\end{aligned} \tag{5.27}$$

3. **Other Options:**

Again, other options as discussed for (5.1) may be pursued.

6. Two-step Explicit Five-Point Finite Volume Schemes.

The grid-point distribution for the domain of dependence of φ_3 as illustrated in Figure 3.2 contains five grid points at the departure time t^{n-1} and so we investigate extensions of the discretizations in Section 5 to include the corresponding five points at time t^{n-1}. The extensions considered are based on the grid-point distributions scenarios described in Figure 6.1 where the centroid value φ_0 is not utilized in updating φ_3 and in Figure 6.2 where φ_0 is utilized in updating φ_3.

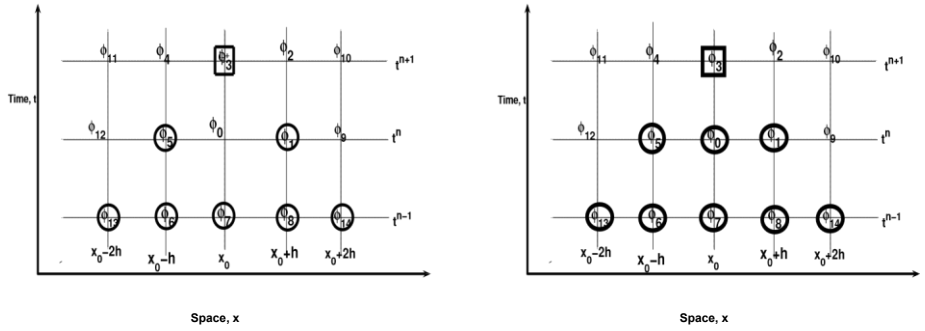

Fig. 6.1. *New update φ_3, is constituted* Fig. 6.2. *New update φ_3, is constituted from a collocation of $\{\varphi_6,\varphi_7,\varphi_8,\varphi_{13},\varphi_{14}\}$ and from a collocation of $\{\varphi_6,\varphi_7,\varphi_8,\varphi_{13},\varphi_{14}\}$ and $\{\varphi_1,\varphi_5\}$ at times t_{n-1} and t_n respectively. $\{\varphi_1,\varphi_0,\varphi_5\}$ at times t_{n-1} and t_n respectively.*

6.1. Temporal and Spatial Leapfrog Integrations. A local accuracy improvement to the approximation of (2.1) by using five quadrature grid points at time t_{n-1} and two points at the current time t_n is described in the parameterized family of schemes by

$$\begin{aligned}\frac{1-2\nu}{2k}\phi_3 = {} & \frac{12(\alpha+\nu)(\phi_6+\phi_8)+(2-3\alpha-9\nu)(\phi_{13}+\phi_{14})-24\nu(\phi_1+\phi_5)}{24k}\\ & +\frac{2(4+9\nu-9\alpha)\phi_7}{24k}-c_0\frac{(4-6\nu)(\phi_1-\phi_5)-(1-6\nu)(\phi_8-\phi_6)}{6h}\\ & +h\frac{(1-6\nu)(\phi_1-\phi_5)-(1-6\nu)(\phi_8-\phi_6)}{6c_0k^2}\\ & +kc_0^2\frac{(3\nu-1)(\phi_{13}+\phi_{14}-2\phi_7)}{12h^2}+F_{52}\end{aligned} \tag{6.1}$$

where F_{52} is the corresponding quadrature discretization of the local source term.

The leading terms of the local residual error which describe the different levels of numerical viscosities associated with the discretization (6.1) are determined as

$$E_{hk} = \left\{ R_4 \frac{\partial^4 \phi}{\partial x^4} + \frac{\nu \sigma^3}{12 c_0^3} \frac{\partial^3 f}{\partial t^3} \right\} h^3 + \left\{ R_5 \frac{\partial^5 \phi}{\partial x^5} + \frac{\nu \sigma^4}{180 c_0^3} \frac{\partial^4 f}{\partial t^4} + g_{31} \frac{\partial^4 f}{\partial x^3 \partial t} + g_{13} \frac{\partial^4 f}{\partial x \partial t^3} \right\} h^4 + O(h^5) \quad (6.2)$$

where

$$R_4 = \frac{c_0}{72\sigma} \left\{ 4(2\sigma^2+1)(\sigma^2-1) - 3\nu(6\sigma^4 - 4\sigma^2 - 5) + 9\alpha \right\},$$
$$R_5 = \frac{c_0}{360} \left\{ (4\sigma^4 + 5\sigma^2 - 9) - 5\nu(2\sigma^4 + 2\sigma^2 - 7) + 15\alpha \right\},$$
$$g_{31} = \frac{\sigma^2(\sigma^2-1)(3\nu-1)}{9c_0}, \qquad g_{13} = \frac{\sigma^2(6\nu(\sigma^2-1) - 2\sigma^2 + 1)}{72 c_0^3}.$$

Notice that the inclusions of $\phi_{13} := \phi_{i-2}^{n-1}$ and $\phi_{14} := \phi_{i+2}^{n-1}$ causes the scheme (6.1) to be dissipative for $\alpha = 0$ and $\nu = 0$ as opposed to scheme (5.2).

As described in the previous sections for the three-point quadrature schemes we discuss similar options for controlling the Gibbs oscillations below.

Strategies to Regulate Nonphysical Oscillations.

1. **Option One:** Clearly, by eliminating both R_4 and R_5 in the residual error (6.2), ν and α are determined as functions of σ by

$$\nu = \left(\frac{7}{30} \frac{4\sigma^2 - 1}{2\sigma^2 - 1}\right), \quad \alpha = \frac{1}{90} \frac{8\sigma^6 + 6\sigma^4 - 72\sigma^2 - 5}{2\sigma^2 - 1} \quad (6.3)$$

where the $R_6 = c_{ik} \frac{(\sigma^2-1)(\sigma^2-4)(4\sigma^2-1)(5\sigma^2+3)}{10080(2\sigma^2-1)\sigma}$, next leading viscosity coefficients become (6.4)

$$R_7 = c_{ik} \frac{(\sigma^2-1)(\sigma^2-4)(4\sigma^2-1)(17\sigma^2+23)}{75600(2\sigma^2 \quad 1)} \quad . (6.5)$$

The leading viscosity coefficients R_6 and R_7 both stay positive by choosing

σ in the ranges $(\frac{1}{2}, 1)$ and $(0, \frac{1}{2})$ and therefore allows for R_6 and R_7 to be regulated to be both positive and small.

2. **Option Two:** On the other hand, the parameters α and ν may be determined as a function of σ to control the size of the viscosity coefficients R_3 and R_4 such that

$$\alpha = 4 \frac{R_4(6\sigma^4 - 4\sigma^2 - 5) - R_3\sigma(2\sigma^4 + 2\sigma^2 - 4)}{c_{ik}(2\sigma^2-1)(\sigma^2-1)} + \frac{1}{90} \frac{8\sigma^6 + 6\sigma^4 - 72\sigma^2 - 5}{2\sigma^2 - 1}$$
$$\nu = \frac{12(R_4 - R_3\sigma)}{c_{ik}(\sigma^2-1)(2\sigma^2-1)} + \frac{7(4\sigma^2-1)}{30(2\sigma^2-1)}, \quad (6.6)$$

where R_3 and R_4 may be chosen to ensure diminishing computational errors.

3. **Other Options:**

By determining α to eliminate just R_4 given as

$$\alpha = \frac{4-10\nu}{9} + \frac{4k^2c^2(2\nu-1)}{9h^2} + \frac{2k^4c^4(9\nu-4)}{9h^4}, \tag{6.7}$$

the leading viscosity coefficients R_5 and R_6 become

$$R_5 = c_{ik}\frac{(\sigma^2-1)(4\sigma^2(15\nu-7)+7-30\nu)}{360} \tag{6.8}$$

$$R_6 = c_{ik}\frac{(\sigma^2-1)(\sigma^4(35\nu-16)-11\nu\sigma^2+1-6\nu)}{360\sigma}. \tag{6.9}$$

Clearly, this option with α as determined in (6.7) allows for choosing ν to control the signs of both R_5 and R_6 to be positive. Additionally, this option with α determined as in (6.7) is very stable for choices of σ in relation to the structure of the leading viscosity coefficients R_6 and R_7 as indicated in (6.4) and (6.5).

6.2. Non-Leapfrog Space and Time Integration. By including the centroid value φ_0 in both temporal and spatial non-leapfrog integrations, a similar version of the scheme (5.14) is derived as

$$\begin{aligned}\frac{1-2\nu}{2k}\phi_3 = {} & \frac{13(\phi_6+\phi_8)-(\phi_{13}+\phi_{14})-21(\phi_1+\phi_5)+(21+90\nu)\phi_7+(42-180\nu)\phi_0}{90k}\\
&+c_0\frac{(8-30\nu)(\phi_1-\phi_5)-(23-30\nu)(\phi_8-\phi_6)+15\rho(\phi_3+\phi_7-2\phi_0)}{30h}\\
&-h\frac{(\phi_1-\phi_5)-(\phi_8-\phi_6)}{15c_0k^2}+kc_0^2\frac{\frac{17-30\nu}{45}(\phi_6+\phi_8)+\frac{\rho}{2}(\phi_8-\phi_6)}{h^2}\\
&-kc_0^2\frac{\frac{3\nu-2}{36}(\phi_{13}+\phi_{14})+\frac{45\nu-26}{30}\phi_7+\frac{30\nu-14}{15}(\phi_1+\phi_5)-\frac{\rho}{2}(\phi_1-\phi_5)}{h^2}\\
&-\rho k^2c_0^3\frac{(\phi_{13}+\phi_{14}+8\phi_6+8\phi_8-18\phi_7)+24(\phi_1+\phi_5-2\phi_0)}{24h^3}\\
&+k^3c_0^4(15\nu-8)\frac{(\phi_{13}+\phi_{14}+4\phi_6+8\phi_8-6\phi_7)}{180h^4}\\
&-\rho k^4c_0^5\frac{(4(\phi_6+\phi_8)-(\phi_{13}+\phi_{14})-6\phi_7)}{24h^5}+F_{522}\end{aligned} \tag{6.10}$$

where F_{522} is the corresponding quadrature discretization of the source term.

The leading terms of the local residual error which describe the different levels of numerical viscosities associated with the discretization (**6.10**) are determined as

$$\begin{aligned}E_{hk} = {} & \frac{\sigma^3(2\nu+\rho\sigma)}{24c_0^3}\frac{\partial^3 f}{\partial t^3}h^3+\left\{\frac{\nu\sigma^4}{180c_0^3}\frac{\partial^4 f}{\partial t^4}+g_{31}\frac{\partial^4 f}{\partial x^3\partial t}+g_{13}\frac{\partial^4 f}{\partial x\partial t^3}\right\}h^4\\
&+\left\{R_6\frac{\partial^6\phi}{\partial x^6}+g_5\frac{\partial^5 f}{\partial t^5}+g_{41}\frac{\partial^5 f}{\partial x^4\partial t}+g_{32}\frac{\partial^5 f}{\partial x^3\partial t^2}+\cdots\right\}h^5+O(h^6)\end{aligned} \tag{6.11}$$

where the associated leading viscosity coefficients are

$$\begin{aligned}R_6 &= \frac{c_0}{3600\sigma}\left\{(1-\sigma^2)(35\rho\sigma^5-36\sigma^4+70\sigma^4\nu+10\rho\sigma^3-7\alpha^2+20\nu\sigma^2+4)\right\},\\
R_7 &= \frac{c_0}{75600}\{(1-\sigma^2)(315\rho\sigma^5-328\sigma^4+630\sigma^4\nu+315\rho\sigma^3-286\alpha^2+630\nu\sigma^2+92)\}.\end{aligned}$$

Nonphysical Oscillation Regulation Strategies. As evident from the functional descriptions of R_6 and R_7, two approaches that may be pursued in regulating the nonphysical oscillations with the discretization (6.10) include determining ν for a given set of feasible values for σ, R_6, R_7, and utilizing choices ρ to control the subsequent leading viscosity coefficients. For instance, consider the following options below:

1. **Option One:** The parameter ν may be determined as a function of σ, ρ and R_6 to control the leading dissipation error coefficient by

$$\nu = \frac{3600R_6\sigma + 11c\sigma^2 - 36c\sigma^6 + 29c\sigma^4 - 10c\sigma^3\rho - 25c\sigma^5\rho + 35c\sigma^7\rho - 4c}{10c\sigma^2(2 - 7\sigma^4 + 5\sigma^2)}, \tag{6.12}$$

where ρ can be chosen given σ to render both R_6 and R_7 to be positive.

2. **Option Two:** On the other hand, ν may be determined as a function of σ, ρ and R_6 to control the leading dissipation error coefficient by

$$\nu = \frac{\rho(315\sigma^7 - 315\sigma^3) - 328\sigma^6 15 + 42c\sigma^4 + 378c\sigma^2 + 75600R_7 - 92c}{630c\sigma^2(1 - \sigma^4)}, \tag{6.13}$$

where choices of σ, ρ and R_6 may be utilized to control R_7 or R_8 etc.

7. Numerical experiments and analysis of schemes. To demonstrate the effectiveness of the quadrature differencing approach for developing efficient spacetime schemes for the scaler conservation laws, we present some of the results of our tests to illustrate local accuracy improvements, conservative skills, and nonphysical oscillations reduction skills of the schemes.

The $p-$norm of the grid function error (global) on Ω at time T, is defined as

$$\|u - \phi\|_p = \left(h \sum_{i=0}^{N} |u(x_i, T) - \phi(x_i, T)|^p \right)^{1/p} \tag{7.1}$$

where $u(x,t)$ is the exact solution at time t and $\varphi(x,t)$ is the space-time numerical approximation of $u(x,t)$ at time t. Thus, $\varphi(x,T)$ is the numerical solution of the of the conservation law (2.1) on Ω at the end of time integration based on a spatial resolution h.

Consider the error e_T based on a spatial resolution of h, measured at the end of a time integration T with the L^∞ norm Ω according to

$$E_{xt} = e_T(h) = \|u - \varphi\|_{L_\infty} = Ch^r + o(h^r) \quad \text{as h} \to 0,$$

where C is independent of h. If h is sufficiently small, then

$$e_T(h) \approx Ch^r, \text{ and } R(h) = \frac{e_T(h)}{e_T(\frac{h}{2})} \approx 2^r$$

where r is the order of accuracy or the convergence rate.

Example 1. To demonstrate the higher level of local conservation and stability associated with the space-time discretization approach through numerical experimentation, consider an initial distribution as the smooth square pulse function

$$g(x) = \frac{1}{1 + \exp\{80(|x - 0.5| - 0.15)\}}, \qquad \Omega = [0,1]$$

as used in the literature to characterize the accuracy of advection schemes [26].

Example 2. In this example, consider the initial condition for the advection equation (2.1) to be

$$\begin{cases} \\ 0 \end{cases} \qquad \begin{array}{l} \text{if} \quad x < t, \\ \text{if} \quad t \le x \le 0.1 \\ \text{if} \quad 0.1 < x \quad 0.5 \end{array}$$

$$h(x) = \begin{cases} \frac{1}{5} & \\ \dfrac{1}{2} & \text{if } 0.5 < x \le 1 \end{cases} \quad \left(\sin^5(\pi x) - 0. \right) \quad \left(1 + \exp(80|x - 0.2| - 0.1) \right) \quad \le$$

consisting of different flow regimes. We investigate the accuracies of handling advection along local characteristics and regularization of the leading viscosity coefficient to control nonphysical oscillations associated with jump discontinuities.

For $f = 0$, the equation (2.1) describes a pure advection and the exact solution is given by $u(x,t) = g(x - ct)$ where $g(x)$ is the initial profile. We demonstrate the accuracies of the advection of g and h in Examples 1 and 2 above with $T = 0.4$ and $c = 1$ by the new schemes as different combinations of the parameters α and ν are utilized to regulate the leading viscosity coefficients of the residual errors for the associated schemes.

In the Figures demonstrating the oscillations reduction skills for the schemes, the resolution is taken as $h = 1/50$ with $c = 1$ and the time steps are calculated according to (3.6).

7.1. Nonphysical Oscillations Reductions. In this section, we discuss spurious oscillations reduction skills of the schemes. The motivation is to develop higherorder accurate schemes that guarantee higher level of computational accuracies and local conservation without the use of flux limiters. Thus, the discretization has to ensure flow accuracies along local characteristics and the space-time design to derive the right collocations of new updates for weighted quadratures of departure points guarantees a more accurate approach to regulate local errors of dispersion and dissipation. Utilizing a general regular distribution of space-time grid-points to approximate the advection equation generates both numerical dispersion and dissipation in the associated residual errors for the schemes. By determining the accurate functional relationships of the leading numerical dispersion and dissipation coefficients with collocation parameters allows for choosing such parameters rightly to minimize the associated errors.

For instance, the second order leapfrog scheme is recovered from the discretization (5.1) with $\nu = 0$ and $\alpha = 0$ and all the dissipative terms in the residual error are eliminated leaving $(1 - \sigma^2)$ as a factor of the coefficient of the dispersive terms. Hence, the spurious oscillations near regions of higher sensitivities may be reduced by choosing σ close to 1 in order to diminish the effects of the leading dissipative terms in the residual error.

On the other hand as discussed and analyzed in Sections 5 and 6, various options for selecting the parameters ν, α, and σ for the numerical schemes presented above including (5.1) may be determined to produce diminishing effects on the dissipative and dispersive coefficients in the respective residual errors.

In Figures 7.1 through 7.4, we demonstrate the accuracies of transporting the smooth square pulse described in Example 1 by the various advection schemes derived above.

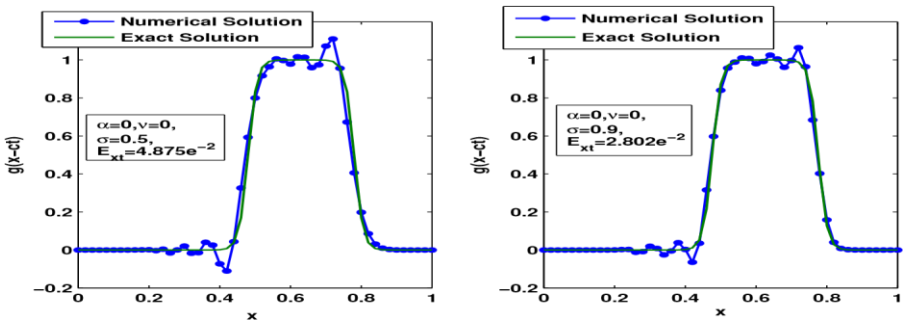

Fig. 7.1. *Nonphysical oscillations regulation and control by scheme (5.1) with* $\alpha = 0$ *and* $\nu = 0$*(Second-order Leapfrog scheme) for left graph, and* $\alpha = \frac{1}{2}$ $\nu = 0$ *for the right. The CFL conditions are maintained at* $\sigma = 0.5$ *for the left with* $\sigma = 0.9$ *for the right with the error* $E_{xt} = \mathrm{ke}_{T,h}\mathrm{k}_2$*, computed by (7.1).*

The graphs in figure 7.1 are the result of advection by the second order leapfrog scheme with $\alpha = 0$ and $\nu = 0$ in (5.1) and both show significant nonphysical oscillations associated with large increases in $\left|\frac{\partial^3 \phi}{\partial x^3}\right|$ and $\left|\frac{\partial^4 \phi}{\partial x^4}\right|$ as indicated by (5.3).

For the stabilized fourth-order leapfrog scheme with the leading coefficient of dispersion as $\frac{(1-\sigma^2)(\sigma^2-4)}{120}$, there is Spurious oscillations with smaller amplitudes as shown in Figure 7.2.

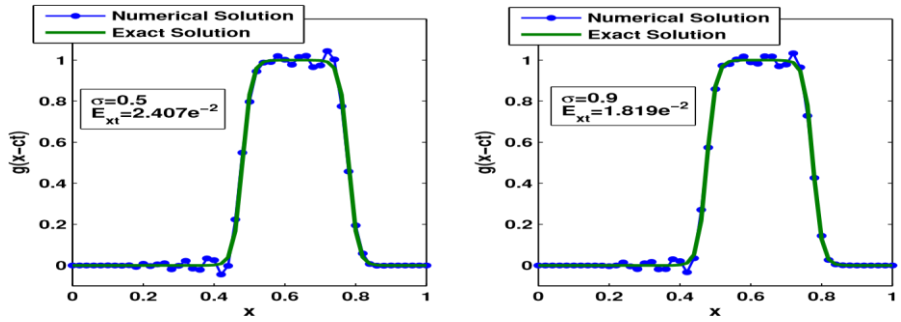

Fig. 7.2. *The stabilized Leapfrog fourth-order scheme still produces the Spurious oscillations with smaller amplitudes.*

However, with alternate choices for $\alpha = 06$ and $\nu = 06$ for the scheme (5.1) the nonphysical oscillations are significantly reduced as demonstrated in Figure 7.3.

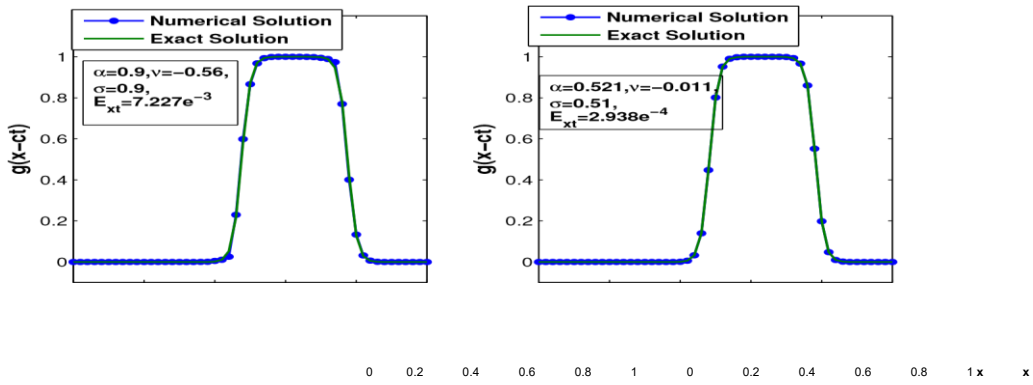

Fig. 7.3. *Nonphysical oscillations regulation and control by the three-point space-time family of schemes (5.1) with* $\alpha = 0.9$ *and* $\nu = -0.56$ *on the left, and* $\alpha = 0.521$ $\nu = -0.011$ *on the right. The CFL conditions are maintained at* $\sigma = 0.9$ *for the left with* $\sigma = 0.51$ *for the right with the error* $E_{xt} = \mathrm{ke}_{T,h}\mathrm{k}_2$*, computed by (7.1).*

Clearly, the spurious oscillations associated with numerical solutions for advection schemes may be controlled by the right space-time collocations of the grid functions in relation to the new updates.

Through similar alternate choices of α and ν, Figure 7.4 demonstrates the skill of reducing the nonphysical oscillation for the third order temporal non-leapfrog scheme (5.14).

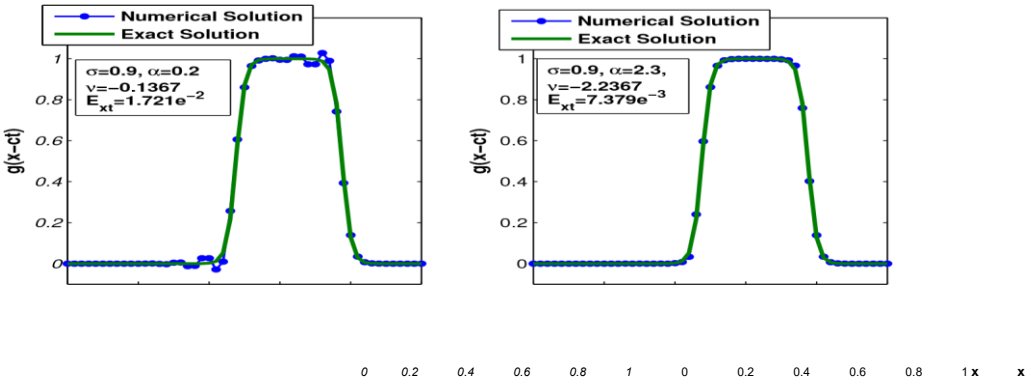

Fig. 7.4. *Nonphysical oscillations regulation and control by the three-point space-time family of schemes (5.14) with* $\alpha = 0.2$ *and* $\nu = -0.1367$ *on the left, and* $\alpha = 2.3$ $\nu = -2.2367$ *on the right. The CFL conditions are maintained at* $\sigma = 0.9$ *for both graphs with the error* $E_{xt} = \mathrm{k}e_{T,h}\mathrm{k}_2$*, computed by (7.1).*

As demonstrated in Figure 7.1 through Figure 7.4, it is clear that the nonphysical oscillations associated with numerical solutions for the advection equation (2.1) may be regulated and effectively controlled for higher-order schemes without flux limiters. By utilizing multiple time steps to constitute new updates, the different courant numbers associated with the different time steps are coupled into the viscosity coefficients through the multivariate space-time expansion of the equation error and hence in the residual errors. Therefore a right averaging choice of a courant number for such numerical solutions may produce diminishing effects on such viscosity coefficients and therefore minimize the errors of dissipation and dispersion.

Through the space-time expansion of the equation error subject to the higherorder derivatives of the equation (2.9), the leading dissipation term in the expansion may be described as the rate of change of the leading dispersion term and vice versa along local characteristics. Therefore the nonphysical oscillations may optimally be controlled and regulated by regulating at least both of the leading coefficients of dissipation and dispersion.

Additionally, by determining the exact functional relationships as illustrated in Figures 5.5 and 5.6, optimal and feasible values for the CFL number σ, the remaining quadrature parameters and sizes of the viscosity coefficients may be determined in the respective schemes to minimize the oscillations in numerical solutions.

As discussed above in the strategies for regulating these oscillations, from Figures 5.5 and 5.6 and equations (5.5) to (5.7), choosing the CFL condition number $\sigma > 0.5$ yields positive values for $R_5(\alpha)$ and $R_6(\alpha)$. Thus, feasible choices of $R_3(\alpha)$ and $R_4(\alpha)$ may then be selected in order to determine the right collocation weights for α and ν according to (5.8) that regulate these leading viscosity coefficients to reduce and minimize the nonphysical oscillations.

For instance, by selecting $\sigma = 0.514$, $R_3 = 7e^{-3}$ and $R_4 = 1e^{-4}$, the quadrature weights α and ν in (5.1) are determined respectively as 0.5008 and −0.015476 according to (5.8) and the numerical solution for the initial condition profile in Example 2 produces the numerical viscosity coefficients $[R_5, R_6, R_7] = [8.124, 0.7004, 0.384]e^{-4}$ and the results are displayed in Figure 7.5.

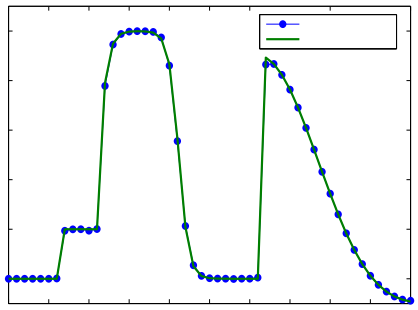

Fig. 7.5. *Nonphysical oscillations regulation and control for scheme (5.1) with* $\sigma = 0.514$*. Leading viscosity coefficients set as* $R_3 = 7e^{-3}$, $R_4 = 1e^{-4}$ *and quadrature weights determined by (5.8) as* $\alpha = 0.5008$ *and* $\nu = -0.015476$*. Error is determined as* $\mathrm{ke}_{T,h}\mathrm{k}_2 = 5.054e^{-3}$ *with computational viscosity coefficients as* $[R_5, R_6, R_7] = [8.124, 0.7004, 0.384]e^{-4}$

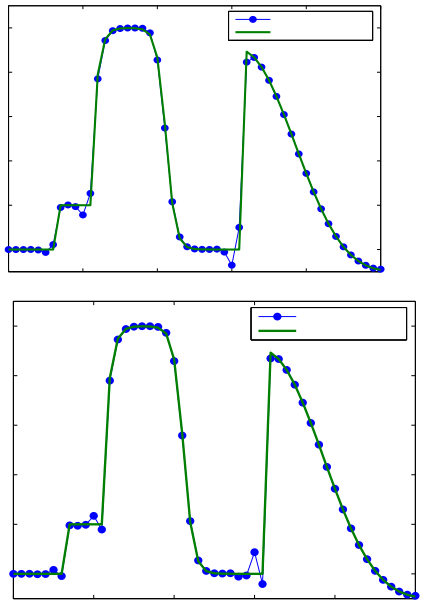

Fig. 7.6. *Nonphysical oscillations regulation and control for scheme (5.1) with* $\sigma = 0.514$*, leading viscosity coefficients in Residual error set as* $R_3 = 1.2e^{-2}$, $R_4 = 1e^{-4}$ *and quadrature weights determined by (5.8) as* $\alpha = 0.4792$ *and* $\nu = -0.014837$, $\mathrm{ke}_{T,h}\mathrm{k}_2 = 2.1745e^{-2}$ *and* $[R_5, R_6, R_7] = [11.138, 0.6754, 0.4528]e^{-4}$

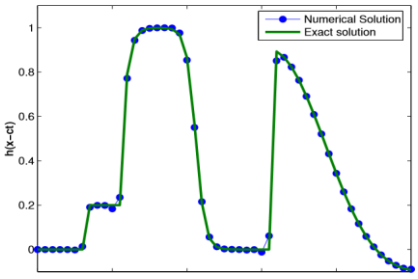

Fig. 7.7. *Nonphysical oscillations regulation and control for scheme (5.1) with* $\sigma = 0.514$*, leading viscosity coefficients in Residual error set as* $R_3 = 7e^{-3}$, $R_4 = 1e^{-3}$ *and quadrature weights determined by (5.8) as* $\alpha = 0.5162$ *and* $\nu = -0.021724$. $\mathrm{ke}_{T,h}\mathrm{k}_2 = 1.558e^{-2}$

$[R_5, R_6, R_7] = [10.943, 1.783, 0.6216]e^{-4}$

Fig. 7.8. *Nonphysical oscillations regulation and control for scheme (5.1) with* $\sigma = 0.514$*, leading viscosity coefficients in Residual error set as* $R_3 = 1.2e^{-2}$, $R_4 = -1e^{-3}$ *and quadrature weights determined by (5.8) as* $\alpha = 0.4947$ *and* $\nu = -0.021085$. $\mathrm{ke}_{T,h}\mathrm{k}_2 = 1.28879e^{-2}$

$[R_5, R_6, R_7] = [13.957, 1.758, 0.6903]e^{-4}$

Figures 7.5 to 7.8 demonstrate the nonphysical oscillation reduction skill for the temporal and spatial leapfrog discretization (5.1) where new updates at time t^{n+1} are

constructed in time from a linear combination of three solution points at time t^{n-1} and two solution points at time t^n without the space-time centroid value.

Good selections for R_3 and R_4 are made based on the profiles from Figure 5.5 and Figure 5.6 which yield significant reductions in the oscillations as shown in Figure 7.5. However, in Figures 7.6 and 7.7 the choice ratios for R_3 to R_4 is slightly different resulting in the reappearance of the oscillations. In Figure 7.8, the oscillations are reduced with larger values for R_3 and R_4 than in Figure 7.5 but with larger ratio.

Next, we discuss in Figures 7.9 to 7.11 the nonphysical oscillation reduction skill for the temporal non-leapfrog discretization (5.14) where new updates at time t^{n+1} are constructed in time from a quadrature of three solution points at both times t^{n-1} and t^n including the space-time centroid value.

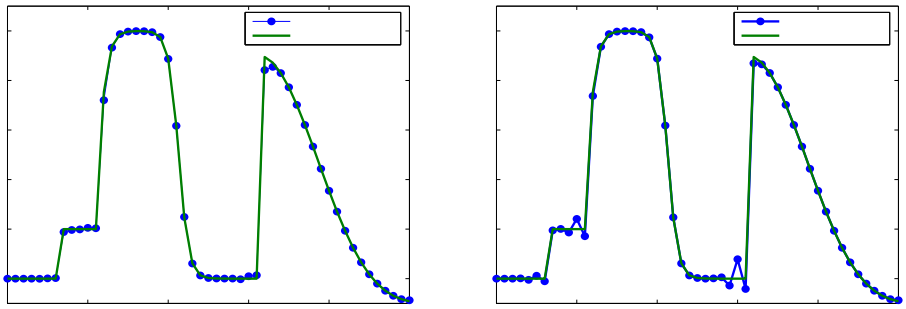

Fig. 7.9. *Reduced and controlled oscillations for scheme (5.14) with* $\sigma = 0.45$, *leading viscosity coefficients in Residual Error set as* $R_4 = 1e{-3}$, $R_5 = 2e{-4}$. $ke_{T,h}k_2 = 1.1579e{-2}$, $[R_6, R_7] = [2.0911, 0.3125]e^{-4}$

Fig. 7.10. *Oscillations appear for scheme (5.14) with* $\sigma = 0.45$, *leading viscosity coefficients in Residual error set as* $R_4 = 1e^{-3}$, $R_5 = -2e^{-4}$. $ke_{T,h}k_2 = 9.6674e^{-3}$, $[R_6, R_7] = [1.0785, -0.0008107]e^{-4}$

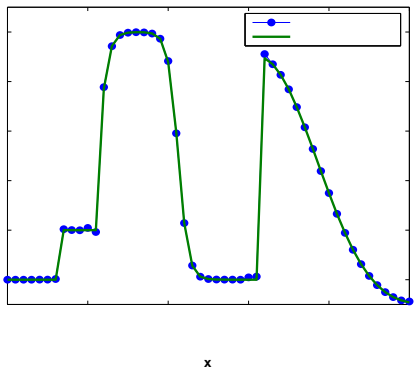

Fig. 7.11. *Reduced and controlled oscillations for scheme (5.14) with* $\sigma = 0.48$, *leading viscosity coefficients in Residual Error set as* $R_4 = -1e{-3}$, $R_5 = -2e{-4}$. $ke_{T,h}k_2 = 3.868e{-3}$,

$[R_6, R_7] = [-4.732, -1.039]e^{-5}$

For the non-leapfrog discretization (5.14), the profile of the viscosity coefficients displayed in Figures 5.7 and 5.8 guide the choices of $\sigma < 0.5$ and approaching $\frac{1}{2}^-$ to maintain desirable small and positive values for

leading viscosity coefficients. In Figure 7.9, both R_4 and R_5 were both set positive with $R_4 > R_5$ which produced significant reductions in the oscillations as well as in Figure 7.11 where both are set negative. The oscillations appear in Figure 7.10 when R_5 is set negative demonstrating that both R_4 and R_5 need to be controlled to reduce the oscillations.

Next, we discuss in Figures 7.12 to 7.14 the nonphysical oscillation reduction skill for the temporal leapfrog discretization (6.1) where new updates at time t^{n+1} are constructed in time from a quadrature of five points at time t^{n-1} and two points at time t^n excluding the space-time centroid value.

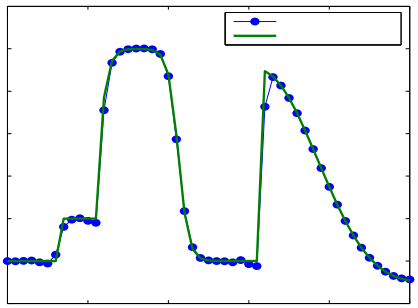

Fig. 7.12. *Reduced and controlled oscillations for scheme (6.1) with* $\sigma = 0.48$, *leading viscosity coefficients in Residual Error set as*

$R_4 = 1e{-}3$, $R_5 = 1e{-}4$. $ke_{T,h}k2 = 2.70e{-}2$,

$[R_6, R_7, R_8] = [2.93, 1.04, -1.42]e^{-4}$

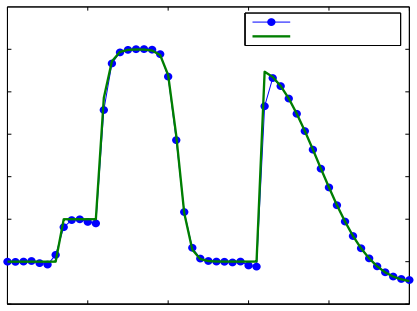

Fig. 7.14. *Reduced and controlled oscillations for scheme (6.1) with* $\sigma = 0.48$, *leading viscosity coefficients in Residual error set as*

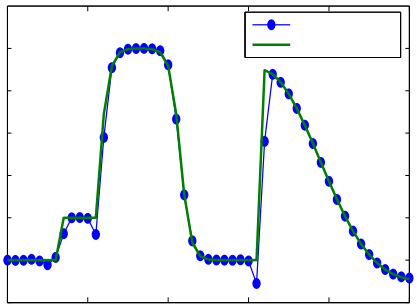

Fig. 7.13. *Oscillations appear for scheme (6.1) with* $\sigma = 0.49$, *leading viscosity coefficients in Residual error set as*

$R_4 = 1e{-}3$, $R_5 = -2e{-}4$. $ke_{T,h}k2 = 3.99e{-}2$, $[R_6, R_7, R_8] = [2.08, 0.667, -0.0592]e^{-4}$

$R_4 = 1e{-}3$, $R_5 = -1e{-}5$. $ke_{T,h}k2 = 2.63e{-}2$,

$[R_6, R_7, R_8] = [1.983, 0.6208, -0.0381]e^{-4}$

For the temporal leapfrog discretization (6.1), the functional profiles of the viscosity coefficients (6.4) and (6.5) guide the choices of $\sigma < 0.5$ and approaching $\frac{1}{2}^-$ to maintain desirable small and positive values for

leading viscosity coefficients.

In Figure 7.12, both R_4 and R_5 were both set positive with $R_4 > R_5$ which produced significant reductions in the oscillations as well as in Figure 7.14 where R_5 is set negative. The oscillations appear in Figure 7.13 when R_5 is set negative with a slight change to $\sigma = 0.49$ demonstrating relative sensitivity for scheme (6.1) and compared to (5.2) and (5.14) for the five-point stencil at time t^{n-1}.

Next, we discuss in Figures 7.15 to 7.17 the nonphysical oscillation reduction skill for the temporal non-leapfrog discretization (6.10) where new updates at time t^{n+1} are constructed in time from a quadrature of five points at time t^{n-1} and three points at time t^n including the space-time centroid value.

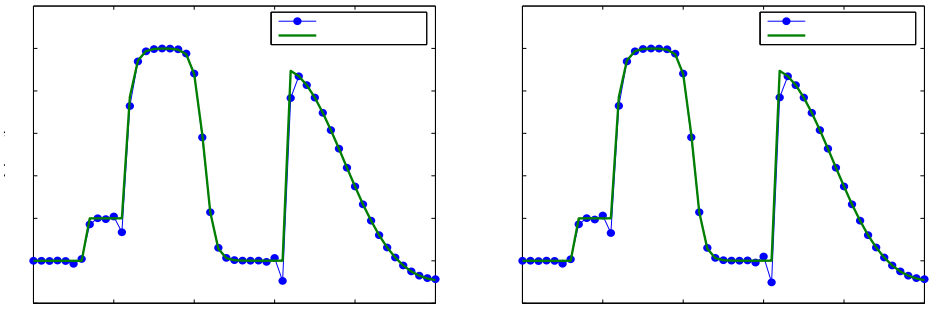

Fig. 7.15. *Nonphysical oscillations regulation and control by scheme (6.10) with* $\sigma = 0.48$. *Leading viscosity coefficient in Residual error set as* $G_6 = 6.6e^{-5}$ *as in (6.12) with* $\rho = 0$ *with numerical results as* $ke_{T,h}k_2 = 2.576e^{-2}$, $[R_6, R_7, R_8] = [6.6, 1.687, 0.1009]e^{-5}$

Fig. 7.16. *Nonphysical oscillations regulation and control by scheme (6.10) with* $\sigma = 0.48$. *Leading viscosity coefficient in Residual error set as* $G_7 = 1.2e^{-5}$ *as in (6.13) with* $\rho = 0$ *with numerical results as* $ke_{T,h}k_2 = 2.60e^{-2}$, $[R_6, R_7, R_8] = [5.61, 1.2, 0.158]e^{-5}$

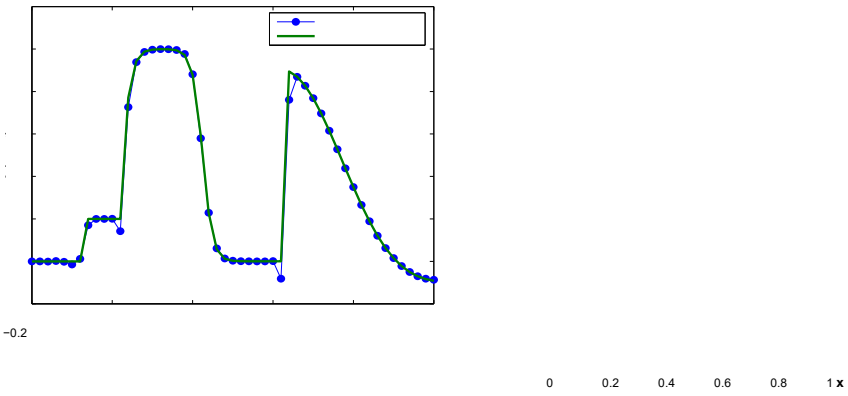

Nonphysical oscillations regulation and control by a different version of scheme (6.10) with $\sigma = 0.48$.

Leading viscosity coefficients G_5 and G_6 similar to other options strategy described for scheme (6.1) are set as $G_5 = 8e^{-6}$, $G_6 = 1.1e^{-4}$, $\rho = 0$. Numerical results as k k R , R , R , R

$e_{T,h}{}_2 = 2.501e^{-2}$, [5 6 7 8] = $[0.8, 11, 3.81, -0.13]e^{-5}$ $_{T,h}{}_2 = 2.57$, [4 5 6 7 8] = $[6.1, -2.1, 0.6, 0.107, -0.299]e^{-4}$

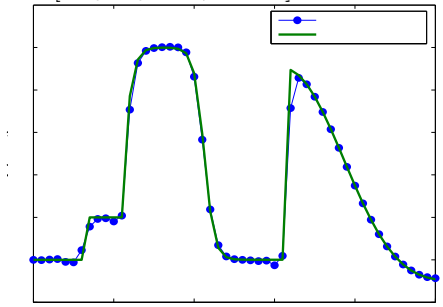

Fig. 7.17. *Nonphysical oscillations regulation and control by another version of scheme (6.10) with* $\sigma = 0.48$. *Leading viscosity coefficients* G_4, G_5 *and* G_6 *similar to other options strategy described for scheme (6.1) are set as* $G_4 = 6.1e^{-4}$, $G_5 = -2.1e^{-4}$, $G_6 = 6.0e^{-5}$, $\rho = 0$. *Numerical results as*

ke k e^{-2} R, R, R, R, R

For the current quadrature description of (6.10), attempts to control the sizes of G_6 and G_7 separately as described in (6.12) and (6.13) lead to similar profiles in Figures 7.15 and 7.16 respectively. By scaling back the order of accuracy to allow for the control both G_5 and G_6 together as described above for the other schemes leads to a similar profile in Figure 7.1. However, by controlling G_4, G_5 and G_6 together leads to reductions in the nonphysical oscillations as displayed in Figure 7.17.

7.2. Grid Refinement Analysis. To demonstrate rate of convergence and accuracy for the schemes, consider the initial distribution as the smooth square pulse function in Example 1 as used in the literature to characterize the accuracy of advection schemes [26].

For $f = 0$, the equation (2.1) describes a pure advection and the exact solution is given by $u(x,t) = g(x - ct)$. In demonstrating the convergence rate and accuracy of the schemes, the relationship between k and h which describes the directions of the characteristics (3.6) is maintained to ensure consistent domains of dependence at finer resolutions.

Experiment 1. In Table 7.1, we present the results of the computational experiments for the three-point compact two-step family of split explicit schemes (5.1) which include the second-order leapfrog scheme with $\alpha = 0$ and $\nu = 0$. As illustrated in Figures 3.1 and 3.2, the grid functions φ_1, φ_5, φ_6, φ_7, φ_8 are all within the domain of dependence of φ_3. Therefore, updating φ_3 from a quadrature of φ_1, φ_5, φ_6, φ_7 and φ_8 where the quadrature weights are indicated in terms α ν have been effective for the convergence rate and accuracy.

	$\sigma = 0.9$		$\sigma = 0.48$		$\sigma = 0.9$		$\sigma = 0.985$	
			$\nu = 0$		$\nu = -\frac{1}{90}$		$\nu = -\frac{1}{50}$	
h			$\alpha = \frac{1}{2}$	rate	$\alpha = \frac{1}{7}$	rate	$\alpha = \frac{1}{25}$	
$\frac{1}{50}$	$2.852e^{-2}$		$5.870e^{-3}$		$1.994e^{-2}$		$4.838e^{-3}$	
$\frac{1}{100}$	$6.379e^{-3}$	2.16	$8.686e^{-4}$	2.76	$3.735e^{-3}$	2.43	$9.389e^{-4}$	2.37
$\frac{1}{200}$	$1.391e^{-3}$	2.19	$1.576e^{-4}$	2.46	$3.087e^{-4}$	3.60	$5.596e^{-5}$	4.07
$\frac{1}{400}$	$3.341e^{-4}$	2.06	$3.742e^{-5}$	2.07	$3.366e^{-5}$	3.20	$6.001e^{-6}$	3.22

$\nu = 0$

$\alpha = 0$ rate rate

Table 7.1

Grid refinement analysis for the three-point leapfrog in time discretization (5.1). Column one describes the Results in column one are for the second order Leapfrog scheme.

Experiment 2. In this experiment, we further examine computational accuracy and convergence when φ_3 is calculated from a wider numerical domain of dependence
[6] of φ_3 consisting of the grid functions φ_{13}, φ_{14}, φ_6, φ_8 and φ_7 at t^{n-1} and φ_1, φ_5, at time step t^{n-1} which are within the numerical domain of dependence.

The first column of Table 7.2 under LF-4 details the results for a new stabilized and improved leapfrog-time fourth-order scheme where advection is calculated at the current time level t^n using the four grid functions

φ_1, φ_5, φ_9 and φ_{12} about the centroid.

h		rate	rate	rate
$\frac{1}{50}$	$1.819e^{-2}$	$1.388e^{-2}$	$9.626e^{-3}$	$1.691e^{-3}$
$\frac{1}{100}$	$1.681e^{-3}$ 3.44	$1.930e^{-3}$ 2.85	$1.888e^{-3}$ 2.35	$3.120e^{-4}$ 2.44
$\frac{1}{20}$	$9.417e^{-5}$ 4.16	$1.462e^{-4}$ 3.72	$6.108e^{-5}$ 4.95	$9.427e^{-6}$ 5.05
$\frac{1}{400}$	$7.399e^{-6}$ 3.67	$1.712e^{-5}$ 3.09	$4.076e^{-6}$ 3.91	$4.063e^{-7}$ 4.54
	$\sigma=0.9$	$\sigma=0.65$	$\sigma=0.96$	$\sigma=0.985$
	IF-4	$\nu=0$ $\alpha=\frac{1}{8}$	$\nu=-\frac{1}{40}$ $\alpha=\frac{1}{8}$	$\nu=-\frac{1}{20}$ $\alpha=\frac{1}{15}$

For the other three columns, advection is calculated using the grid functions φ_1, φ_5, at the t^n time level and φ_6, φ_8 at the t^{n-1} time level. The new update φ_3, is constituted from a linear combination of five grid point functions at t_0-k as described in (6.1).

Table 7.2

Grid refinement analysis for the Five-point leapfrog discretization scheme (6.1).

8. Convergence analysis of schemes. To discuss stability and accuracy of the schemes, we describe the set up of the fully explicit space-time finite volume discretization (3.3) about the centroid as

$$\phi_j|_{t_{n+1}} = \sum \alpha_i \phi_i|_{t_n} - \sum \beta_i \phi_i|_{t_{n-1}} + c_0 \left\{ \sum a_i \phi_i|_{x_0+a_h h} - \sum b_i \phi_i|_{x_0-a_h h} \right\} + \sum_{i=0}^{n_v} v_i f_i + R_{ik} \qquad (8.1)$$

where the weights α_i, β_i, a_i, b_i and v_i are to be determined as functions of h, k and n_v is the total number of the cloud of grid points adopted for collocating the local source term on each control volume with R_{ik} as described in (3.8).

To achieve consistent higher order accuracies for the schemes, the local discretization must be effective and consistent for the equation (3.3) such that

$$\sum a_i = \sum b_i, \quad \alpha_i = 1, \text{ and } v_0 = 1 - \sum v_i. \qquad (8.2)$$

The requirement (8.2) enforces local conservation of φ such that incoming and outgoing fluxes are balanced out and enforced through the minimization process of the local discretization error about the centroid.

The levels of local flux conservation and hence accuracy depend of the size of the local grid point cloud as illustrated above in Tables 7.1 and 7.2 where five-point discretization guarantees improved accuracy over three-point discretization. Furthermore, the collocation parameters α_i in (8.1) describe the relative influences of the grid functions within the numerical domain of dependence at the current time step and which must be wide enough to contain the analytical domain of dependence of the PDE [6,16].

In formulating the space-time discretization error as described, the space-time coefficients of the dissipative and dispersive terms in the error are completely characterized in terms of the collocation parameters.

Thus instead of discretizing such derivative terms to render the schemes diffusive, the collocation weights are optimally determined to minimize the effects of such coefficients similar to vanishing viscosity approaches as demonstrated in computational experimentations in Section 7. The multivariate space-time formulation of the error ensures accurate coupling between spatial and temporal differencing to prevent grid splitting and the associated spurious computational mode. As a result, the schemes include additional terms that describe grid function communications between the initial time and the time-stepping levels.

9. Conclusion. We have demonstrated the effectiveness of using the finite volume method to develop new effective higher-order space-time explicit schemes for scaler conservation laws capable of utilizing associated viscosity coefficients in controlling nonphysical oscillations in numerical solutions. The uniform distributions of grid-point clouds guarantees effective local higher order accuracy through efficient methods of conserving fluxes locally. By using multivariate space-time expansions to approximate the solution and the source term locally, higher-order accuracies along characteristics are ensured by determining and then regulating the accurate descriptions of the leading viscosity coefficients in the space-time residual error. Conditions for stability, accuracy and convergence may be established based on these closed form descriptions of the viscosity coefficients and the residual error.

REFERENCES

[1] C. L. Bottasso. On the computation of the boundary integral of space-time deforming finite elements. *Comm. Numer. Meth. Engrg.*, 13:53–59, 1997.

[2] B. Diskin and J. L. Thomas. Accuracy analysis for mixed-element finite-volume discretization schemes. *NIA Report NO. 2007-08*, 2007.

[3] D. A. French. A space-time finite element method for the wave equation. *Comput. Methods. Appl. Mech. Engrg.*, 107:145–157, 1993.

[4] S. Gabersek and D. R. Durran. Gap Flows through Idealized Topography. Part II: Effects of Rotation and Surface Friction. *J. Atmos. Sci.*, 63:2720–2315, 2006.

[5] J.L. Guermond, R. Pasquetti, and B. Popov. Entropy viscosity method for nonlinear conservation laws. *J. Comput. Phys.*, 230:4248–4267, 2011.

[6] M. T. Heath. *Scientific Computing, An Introductory Survey*. McGraw-Hill, New York, 2002.

[7] K. Ito, Y. Kyei, and Z. Li. Higher-Order, Cartesian Grid Based Finite Difference Schemes for Elliptic Equations on Irregular Domains . *SIAM J. Sci. Comput.*, 27:346–367, 2005.

[8] C. Katz and A. Jameson. A Comparison of Various Meshless Schemes Within a Unified Algorithm. *47th AIAA Aerospace Sciences Meeting including The New Horizons Forum and Aerospace Exposition*, 2009-897, 2009.

[9] E. P. C. Koh, H. M. Tsai, and F. Liu. Euler Solution Using Cartesian Grid with a Gridless Least-Squares Boundary Treatment. *AIAA Journal*, 43(2), 2005.

[10] Y. Kyei. Space-time finite volume differencing framework for effective higher-order accurate discretizations of parabolic equations. *SIAM J. Sci. Comput.*, 34(3):A1432–A1459, 2012.

[11] Y. Liu, M. Vinokur, and Z.J. Wang. Spectral (finite) volume method for conservation laws on unstructured grids V: Extension to three-dimensional systems. *J. Comput. Phys.*, 212:454– 472, 2006.

[12] F. Lorcher, G. Gassner, and C. D. Munz. An explicit discontinuous Galerkin scheme with local time-stepping for general unsteady diffusion equations. *J. Comput. Phys.*, 227:5649–5670, 2008.

[13] Y. Lv, Y. C. See, and M. Ihme. An entropy-residual shock detector for solving conservation laws using high-order discontinuous galerkin methods. *J. Comput. Phys.*, 322:448–472, 2016.

[14] C. Mattiussi. The finite volume, finite element, and finite difference methods as numerical methods for physical field problems. *Advances in Imaging and Electron Physics*, 113:1– 146, 2000.

[15] C. Mattiussi. The Geometry Of Time-Stepping. *Progress In Electromagnetics Research*, PIER 32:123–149, 2001.

[16] F. Messenger and A. Arakwa. *Numerical methods in atmospheric models*. GARP Publications Series No. 17, New York, 1976.

[17] S. Mittal and T.E. Tezduyar. Notes on the stabilized space-time finite-element formulation of unsteady incompressible flows. *Comput. Phys. Commun.*, 73:93–112, 1992.

[18] E. Onate and M. Manzan. A general procedure for deriving stabilized space-time finite element methods for advective-diffusive problems. *Int. J. Numer. Meth. Fluids*, 31:203–221, 1999.

[19] M. Piller and E. Stalio. Finite volume compact schemes on staggered grids. *J. Comput. Phys.*, 197:1064–1094, 2004.

[20] M. Restelli, L. Bonaventura, and R. Sacco. A semi-lagrangian discontinuous galerkin method for scalar advection by incompressible flows. *J. Comput. Phys.*, 216:195–215, 2006.

[21] J. Santos and P. de Oliveira. A converging finite volume scheme for hyperbolic conservation laws with source terms. *J. Comput. App. Math.*, 111:239–251, 1999.

[22] V.A. Titarev and E.F. Toro. ADER Schemes For Hyperbolic Conservation Laws With Reactive Terms. *J. Comput. App. Math.*, 111:239–251, 1999.

[23] E.F. Toro and V.A. Titarev. Derivative Riemann solvers for systems of conservation laws and ADER methods. *J. Comput. Phys.*, 221:693–723, 2006.

[24] A. K. Verma, S. M. Bhallamudi, and V. Eswaran. Overlapping control volume method for solute transport. *J. Hydr. Engrg.*, 5:308–316, 2000.

[25] E. Weinan and B. Engquist. Multiscale Modeling and Computation. *Notices Of The AMS*, 50(9):1062–1070, 2003.

[26] L. J. Wicker and W. C. Skamarock. Time-Splitting Methods for Elastic Models Using Forward Time Schemes. *Mon. Wea. Rev.*, 130:2088–2097, 2002.

[27] M. L. Yu, F. X. Giraldo, and M. Pengand Z. J. Wang. Localized artificial viscosity stabilization of discontinuous galerkin methods for nonhydrostatic mesoscale atmospheric modeling. *J. Comput. Phys.*, 143, 2014.